Cyclic Shear Response of Fine-Sand Tailings Using Cyclic Direct Shear Test

BY
PRASHANT KHEDOE

TU Delft
Delft University of Technology

Cyclic Shear Response of Fine-Sand Tailings Using Cyclic Direct Shear Test

By

Prashant Khedoe

Master thesis submitted to Delft University of Technology in partial fulfilment of the requirements for the degree of

Master of science
in Applied Earth Sciences

to be defended publicly on Tuesday June 28, 2022 at 12:00 PM.
Faculty of Civil Engineering & Geosciences

Student number: 4092201

Thesis committee:

Dr. P.J. Vardon (Chair)	TU Delft, Geo-engineering
A. Golchin	TU Delft, Geo-engineering
Dr. Ir. R.C. Lanzafame	TU Delft, Hydraulic structures & floodrisk
Dr. S. Muraro	TU Delft, Geo-engineering

Abstract

The extraction and processing of mineral and metal ores in the mining industry comes paired with large amounts of mine waste, also known as tailings. This waste consists of various chemicals, acids, and heavy metals which are used during these extraction processes. The tailings are usually stored off in tailings storage facilities (TSF) in a loose state, gradually consolidating over time. TSFs founded in seismically active areas are susceptible to liquefaction due to earthquake loading. Historic data show that about 35% of dam failures are due to liquefaction of the tailings, thus increasing the need to study the liquefaction responses of tailings under cyclic loading. Extensive studies have already been conducted using cyclic direct simple shear (DSS) and cyclic triaxial (CTX) tests as these tests under constant-volume conditions can evaluate the change in pore pressure within a soil accurately. Previous study shows what importance the relative density and sloping ground conditions, known as drained shear bias, have on the cyclic resistance to liquefaction of the tailings. However, in practice the pore water is not bounded within the material and excess pore water can flow out through installed drains.

A round-robin program, issued by the University of Western Australia (UWA), requested a study on the liquefaction response of a particular fine-sand tailings material. Inspired by this round-robin program, an interest raised in studying the cyclic shear response of tailings by using a direct shear box to investigate the cyclic behaviour under partially drained conditions. With use of the direct-shear apparatus of Wille Geotechnik, a test program has been set up to study the influences of relative density and drained shear bias under stress-controlled cyclic shearing and under constant normal load conditions.

Results of the experiments met the expectations that denser soils have a 9.6% higher cyclic resistance ratio (CRR), and samples with applied drained shear bias have a 32% lower CRR compared to samples tested with level ground conditions. Furthermore, samples which underwent post-cyclic shearing showed strain-hardening responses and yielded higher shear stresses compared to the monotonic test, indicating that the constant normal load further densified the samples during cyclic shearing. However, during the experiments, it was quickly found out that the loading frequency was not being applied optimally making it not possible to analyse influence of partially drained conditions . This study showed promise on its capabilities to study cyclic shear loading on a soil. For future work, it is suggested to perform similar tests under a uniform loading frequency with the use of a shear box to evaluate its capabilities to study on partially drained conditions. It is also recommended to conduct tests under constant volume conditions, to evaluate the shear-box apparatus' capabilities to study the liquefaction response of a soil due to excess pore pressure generation.

Acknowledgements

This Msc thesis marks my final stop as student at Delft University of Technology. It has been a long journey with a lot of ups and downs, especially during the COVID-19 period. Nonetheless, I have learned and improved a lot in both my research- and communication skills, and this period also showed me that I can still improve. And like all thesis projects, this journey was not possible to do alone.

First and foremost, I would like to thank my chair supervisor, Phil Vardon for introducing me to this topic and giving me the opportunity to graduate in his group. His knowledge about soil mechanics and advice of how to approach certain aspects of this thesis helped me a great deal in writing my thesis. Furthermore, I would like to thank Ali Golchin, my daily supervisor, for the numerous meetings, both online and in person. Our frequent brain storming sessions gave shape to the objective of this thesis and the discussion of the laboratory results leading to some insightful hypotheses. His encouragement also enabled me to think more independently and be more confident in myself, which I will gladly take with me in my future endeavours. I would like to express my sincerest gratitude to the other members of my thesis committee, Stefano Muraro and Robert Lanzafame, for agreeing to join my committee and providing me with their constructive and detailed feedback. This helped me elevate my thesis to a higher level.

I would also like to thank Yimu Guo, a former PhD researcher, who took the time to show me how the Direct Shear apparatus and the accompanied software worked. Also, a special thanks goes to Wille Geotechnik, the manufacturer of the Direct Shear apparatus, for providing me with the specialized license to perform my experiments. I would also like to thank the organizer of the round-robin program at the University of Western Australia for providing the fine-sand tailings.

A special thanks goes to all my friends for their support. Lastly, and most importantly I would like to say thank you to my family, my siblings and my parents, for their continuous and unconditional support throughout my studies.

I wish you a pleasant reading experience and hope you enjoy it as much as I have enjoyed writing it!

Prashant Khedoe
Delft, June 2022

Contents

List of Figures

List of Tables

Chapter 1

Introduction

1.1 Background and motivation

The mining industry is a very important part of the economy, due to the high demand of minerals and metals which are used to produce other industrial and consumer products. However, extracting these metals from ores also produces a large amount of mine waste. This has made waste disposal management a key focus of mining companies. During the extraction processes, chemicals, acids, and heavy metals, among others, are used which get mixed with the mineral processing waste (Seidalinova, 2014). The safe disposal of mine waste necessitates careful consideration of a variety of physical, chemical, and environmental factors. The waste is produced in the form of fine-grained water-sediment slurry, also known as *tailings* (Lottermoser, 2010). Most tailings are usually stored in so-called tailings dams, as depicted in Figure 1.1 in a saturated, loose state, undergoing gradual consolidation over time. Under these conditions, the tailings are susceptible to liquefaction due to earthquakes undergoing shear deformations, especially in seismically active areas. Failure of these dams can lead to catastrophic consequences, endangering the safety of residents living downstream and the facilities. (Ke et al., 2019).

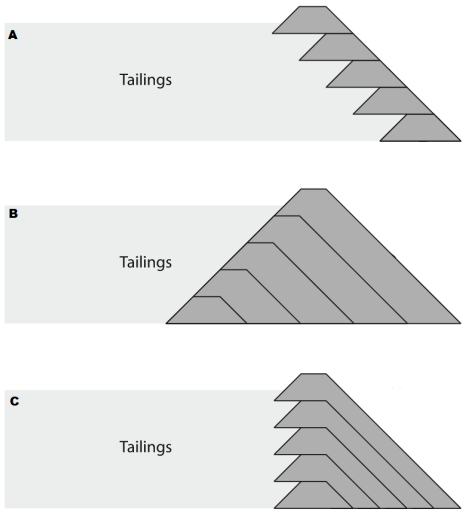

FIGURE 1.1: Construction types of tailings dams: a) Upstream method, b) Downstream method, and c) Center line method.(Modified Figure from Lottermoser, 2010)

Some of the earliest recorded tailings dams failures are El Teniente copper mine (Chile) due to an earthquake in 1928, an old dam at El Cobre copper mine (Chile) following an earthquake in 1965, and a tailings dam failure in Mochikoshi storage lagoon in Japan also due to an earthquake which occurred in 1978 (Ishihara et al., 1980, Lottermoser, 2010). A more recent tailings dam collapse was the 2019 Brumadinho iron mine in Brazil,which took the

lives of 259 people along with major environmental impacts (Silva Rotta et al., 2020). Looking at the causes of tailings dam failures between 1915 and 2016, an estimated 35% of these failures is the cause of liquefaction, thus making liquefaction the main reason for tailings dam failures (Ingabire, 2019). Liquefaction is defined as a phenomenon where saturated soil loses its strength and stiffness due to degradation under monotonic or cyclic loading (Khashila et al., 2021).

The increasing cases of tailings dams failures due to earthquakes raised the importance of investigating the cyclic response of tailings under cyclic loading. This cyclic loading behaviour generate excess pore pressure and decreases the effective stress of the soil. Direct simple shear (DSS) tests and cyclic triaxial (CTX) tests are the most commonly used laboratory tests to mimic the seismic loading behaviour for liquefaction investigation(Khashila et al., 2021). The DSS test can simulate a realistic plane strain condition that involves rotation of principle stresses, while allowing the application of static shear to represent sloping ground conditions. Furthermore, it is also capable of replicating ground conditions during cyclic loading due to an earthquake (Konstadinou et al., 2020). The test allows cyclic variation of the shear stresses in addition to the simultaneous changes of the principle shear stress direction, thus simulating the cyclic rotation of the principle stresses during seismic loading (Wijewickreme et al., 2005). In a cyclic direct simple shear (CDSS) test, the soil sample is subjected to an initial vertical effective stress. To mimic sloping ground conditions in the lab tests, the samples are pre-sheared, also known as drained shear bias, prior to the cyclic test. After the initial stress conditions are applied, the cyclic test is performed stress-controlled under undrained and constant-volume conditions until the liquefaction criteria is reached (Seidalinova, 2014, Wijewickreme et al., 2005, Sanin, 2010). In a CTX test, the soil sample is first isotropically consolidated to a predetermined initial mean effective stress followed by a deviatoric stress (Amini et al., 2000, Khashila et al., 2021).

However, there is limited research done on investigating the cyclic behaviour of tailings using the direct shear test method. The direct shear test is mostly used to determine the consolidated drained strength properties of a soil specimen, with a predetermined failure plane, rather rapidly due to the short drainage paths through the samples, allowing excess pore pressure to dissipate faster than other drained stress tests (ASTMD3080, 2011). In contrast, in a DSS test, the samples deforms with no predetermined failure plane. The shearing behaviour of a specimen using DSS test and direct shear test is visually compared in Figure 1.2. Although, cyclic direct shear (CDS) tests have been performed by researchers, such as Al-Douri et al., 1992 and Cabalar et al., 2013, these tests focused on investigating the strength degradation of soils by the means of strain-controlled tests.

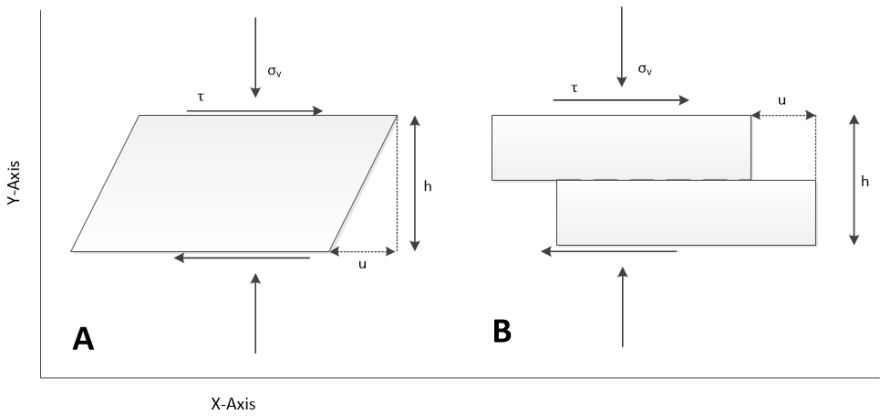

FIGURE 1.2: Difference in shearing of a sample in a direct simple shear apparatus (A) and a direct shear apparatus (B), respectively.

1.2 Objective and scope of the thesis

The objective of this thesis is to investigate the cyclic response of tailings in partially drained conditions by using the *Fully Automatic Electromechanical Direct-Residual Shear Apparatus* of Wille Geotechnik, in the Geo-engineering laboratory at TU Delft. Furthermore, this thesis serves as part of a round robin program, issued by The University of Western Australia (UWA) thus, the scope this thesis mainly includes the requirements of the test program, which are:

- Performing cyclic direct shear tests on dense and loose prepared samples
- Assessing the cyclic shear behaviour of the samples under a certain drained shear bias
- Assessing the effect of the drained shear bias on the relationship of the cyclic resistance ratio (CRR) and void ratio of the specimens

Based on these requirements and the limited research conducted on the study of liquefaction using direct shear test, the following research question is identified: **"How useful is the cyclic direct shear test to study the liquefaction response of fine-sand tailings?"**

To help answer this question the following sub questions are formulated:

1. What is the influence of relative density to reach liquefaction criteria under cyclic direct shear loading?
2. How does the drained shear bias influence the cyclic shear response?
3. How does the fine sand tailings respond when subjected to post-cyclic loading?

1.3 Outline

The structure of the thesis is as follows:

Chapter 2 presents the literature review on cyclic and post-cyclic behaviour of soils and the main factors influencing the cyclic resistance of soils.

Chapter 3 describes the material properties, test procedure, and the test program followed for the laboratory tests.

Chapter 4 presents the results of the experimental tests.

In chapter 5, the discussions and conclusions of the results are explained along with the answers to the research questions.

Finally, chapter 6 presents the recommendations for future research.

Chapter 2

Literature Review

2.1 Monotonic Shear Loading Response

Mechanical responses of sands have been studied by many researchers throughout the years, thus it can be confirmed that the shear stress strain response of sand is primarily governed by relative density and effective confining stress (Verma, 2019). Loose sand samples contract during shearing and the displacement increases with increasing shear stress until eventually an ultimate shear strength is reached. Whereas dense sand samples initially contracts, but dilate afterwards during shearing. First, a peak strength is reached, but with further shearing, the shear resistance drops to the same level as the shear strength of the loose sample. Both of these samples reaches a common steady state volume and it is referred to as the critical void ratio (Casagrande, 1975). This phenomenon is depicted in Figure 2.1.

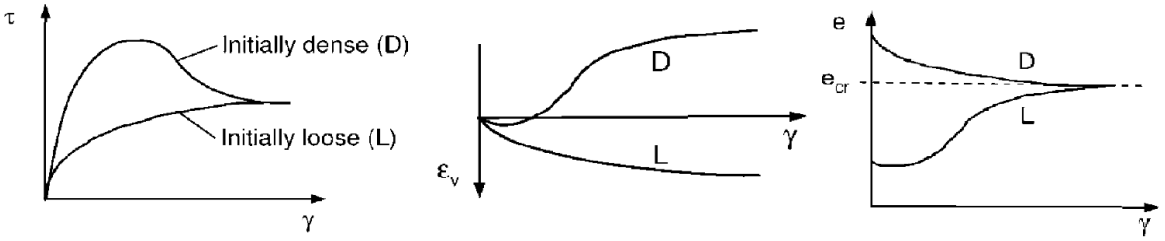

FIGURE 2.1: Comparison of shear stress vs. displacement for loose and dense sand. (Modified Figure from (Randolph et al., 2017))

2.2 Cyclic Shear Loading Response

The liquefaction triggering properties of cohesionless soils are often evaluated using undrained or constant volume cyclic direct simple shear (CV-CDSS) tests (Ulmer et al., 2019). Another method is constant vertical stress method, where the sample is saturated using back-pressure saturation to de-air the samples (Ulmer et al., 2019). The constant vertical stress method often requires more work due to the extra steps of back-pressure saturation and is considered to be more time consuming due to the consolidation step. In contrast, the CV-CDSS method does not require saturated samples or pore pressure measurement; the change in vertical effective stress during cyclic loading is approximately equal to the change in pore pressure that would develop in saturated conditions (Finn et al., 1977, Ulmer et al., 2019). CV-CDSS method is widely used due to its simplicity, in addition to its results being considered to be a more accurate representation to field conditions (Ulmer et al., 2019). The principle stress rotation that occurs during the CDSS tests is comparable to the rotation of principle stresses that take place during earthquake loading (Wijewickreme et al., 2005).

2.2.1 Cyclic shear loading behaviour using direct simple shear (DSS) test

A typical response of CV-CDSS test is shown in Figure 2.2. Wijewickreme et al., 2005 conducted a series of CDSS tests on fine-grained mine tailings and observed a cumulative decrease in effective stress with increasing number of cycles, along with progressive degradation of shear stiffness of the samples under different cyclic stress ratios (CSR = τ_{cyc}/σ'_{vc}). This is referred as "cyclic mobility". Cyclic mobility is the response which exhibits gradual increase in shear strains along with gradual build-up of excess pore water pressure with increasing number of cycles (Seidalinova, 2014).
Various papers considers liquefaction to be triggered in a specimen, subjected to cyclic loading, at 3.75% single-amplitude (SA) shear strain (γ), as it corresponds with achieving 100% excess pore pressure ratio (Ingabire, 2019, Boulanger et al., 1995). In other words, liquefaction is supposed to be triggered in the number of cycles it takes for the specimen to reach a shear strain of 3.75%. An example of this is given in Figure 2.3 for laterite tailings specimens, consolidated under the vertical effective stresses σ'_{vc} = 100kPa and σ'_{vc} = 200kPa.

Cyclic loading may reduce the bearing capacity of a soil and the bearing capacity under cyclic loading may be lower than the capacity under monotonic loading (Andersen, 2009), as shown in Figure 2.4. Andersen, 2009 argues that the reason why the cyclic capacity is smaller than the monotonic capacity is that cyclic loading tends to break down the soil structure and cause volumetric reduction in the soil.

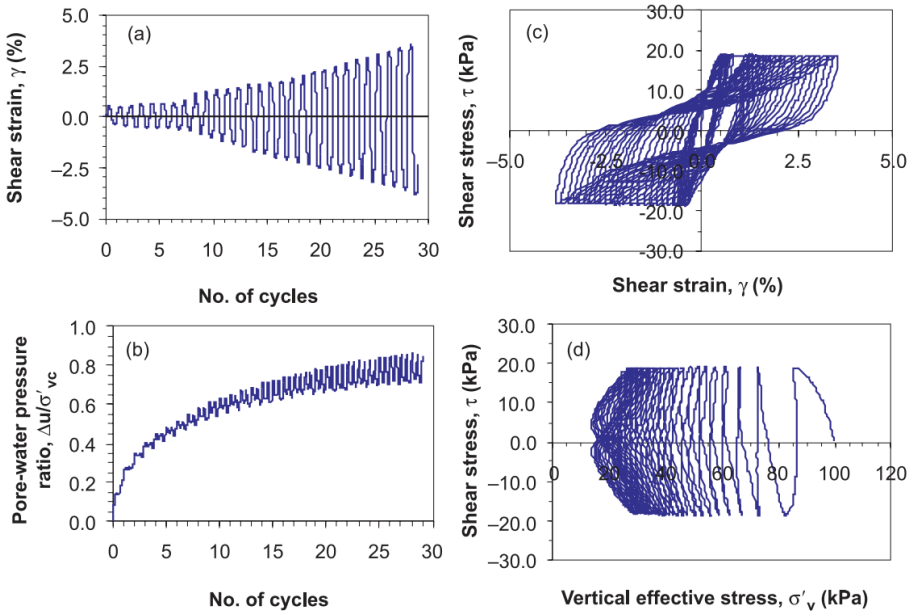

FIGURE 2.2: Typical response of CV-CDSS test on copper-gold tailings, performed by Wijewickreme et al., 2005. a) shear strain development against the number of cycles, b) excess pore-pressure accumulation against the number of cycles, c) stress-strain response, and d) stress-path response.

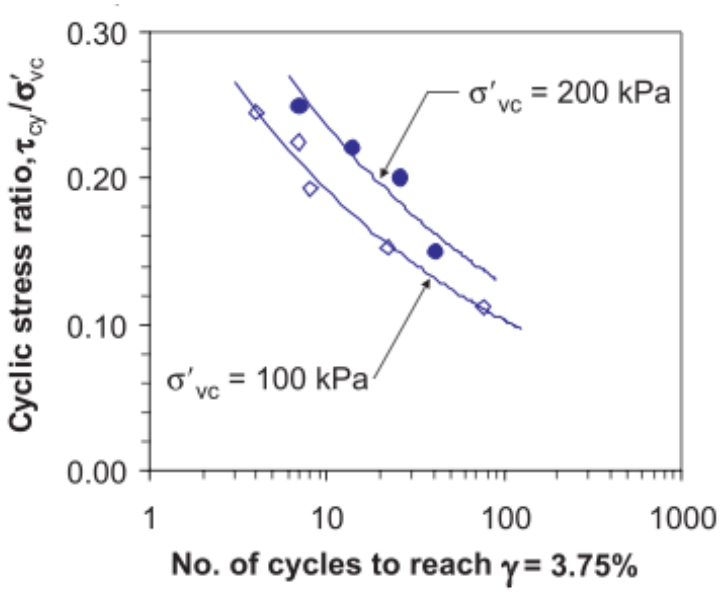

FIGURE 2.3: Relationship of the CSR and the number of cycles to reach γ = 3.75% of tailings samples under two different confining pressures (Wijewickreme et al., 2005).

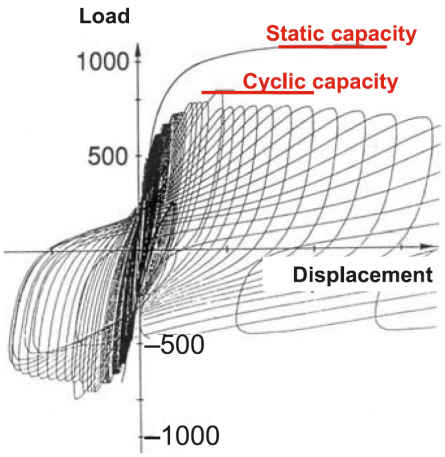

FIGURE 2.4: Comparison of monotonic and cyclic loading response of clay (Andersen, 2009).

2.2.2 Shear loading behaviour using cyclic direct shear (CDS) tests

Cyclic direct shear tests have been conducted to study the shear strength of soil under cyclic conditions. Strain-controlled cyclic direct shear tests have been done by Cabalar et al., 2013 to primarily study the effects of shape of the grains.Their results, as displayed in Figure 2.5, show that the shear stress of the soil increases with increasing applied normal stresses. For silica and calcareous sands, the normal stress, cyclic horizontal displacement, and void ratio all influence the reduction in shear stress during cyclic loading, but particle size and shape also play a role in calcareous sand (Al-Douri et al., 1992). Al-Douri et al., 1992 also concluded that with increasing numbers of cycles, the shear stress reduces, but the rate of change in shear stress also decreases. Furthermore, they concluded that with increasing void ratio, the rate of shear stress reduction also slows down.

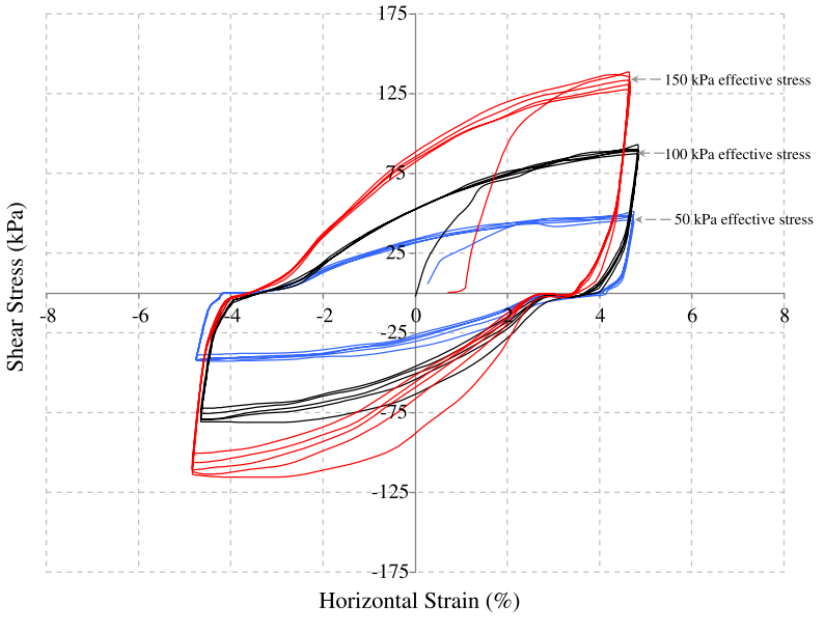

FIGURE 2.5: Cyclic direct shear test response of Narli sand under different normal stresses (Cabalar et al., 2013).

2.3 Post-cyclic Loading

Post-cyclic loading tests are used to determine the residual strength of a soil after cyclic loading. This is done because after a soil has undergone cyclic loading, it may not have enough strength to sustain an existing load (Ingabire, 2019). Wijewickreme et al., 2005, indicates that constant-volume DSS test provides the best estimate of the post-cyclic strength, because this test corresponds to the predominant mode of deformation in the field. Figure 2.6 gives the post-cyclic monotonic response of laterite tailings. Here $S_u - PC$ is the post-cyclic maximum undrained shear strength. Wijewickreme et al., 2005 noted that with increasing strain levels, the specimens showed a dilative behaviour with increasing shear stiffness, until the shear stiffness drops to a plateau at large strains.
Figure 2.7 depicts the relation ship between the post-cyclic maximum shear strength ratio and the consolidated void ratio, obtained from constant-volume monotonic DSS tests (Wijewickreme et al., 2005). The shear strength ratio appears to increase with a decrease in the void ratio. Sivathayalan, 1994 found that the resistance to liquefaction decreased with increasing stress level, for a given void ratio. This effect of stress level increases with relative density.

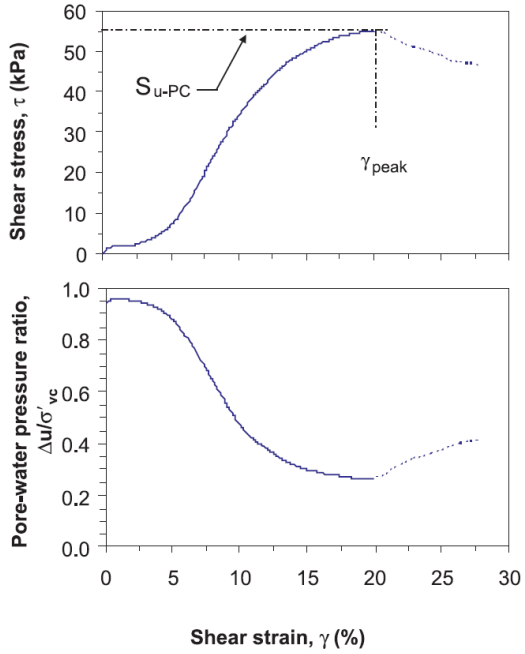

FIGURE 2.6: Post-cyclic monotonic DSS test response of laterite tailings (Wijewickreme et al., 2005).

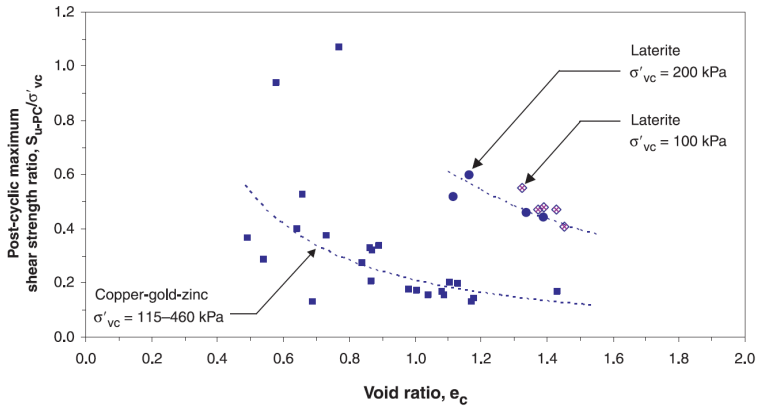

FIGURE 2.7: Relationship between the post cyclic maximum shear strength and the consolidation void ratio (Wijewickreme et al., 2005).

2.4 Cyclic Resistance Ratio (CRR)

The resistance of a soil under cyclic loading is expressed by the cyclic resistance ratio (CRR), which is defined as the relationship between the CSR and the number of cycles required to reach liquefaction for that given CSR (Ulmer et al., 2019, Ingabire, 2019). This number of cycles achieved in the laboratory tests corresponds with the equivalent uniform number of cycles which represents an earthquake with a moment magnitude of M = 7.5. This magnitude is represented with 15 cyclic loading in sands (Sanin, 2010). CRR denotes the capacity of a soil to resist liquefaction. If the CSR caused by an earthquake is higher than the CRR of in-situ soil, then liquefaction could occur during an earthquake (Seidalinova, 2014). Sanin, 2005, Wijewickreme et al., 2005 observed that under high CSR values, the specimens reached an excess pore pressure ratio of 100% or the liquefaction criteria in less number of cycles, than those subjected to lower CSR. Sanin, 2010 noted that the cyclic

resistance in sands generally increase with increasing density for a given relative density, and the cyclic resistance decreases with increasing confining stress.

Ingabire, 2019 indicates that CRR and the number of cycles to liquefaction can be plotted. The curve of this relationship can be plotted as a semi-logarithmic plot and can be expressed with Equation 2.1.

$$CRR = a\left(N_{\gamma=3.75\%}\right)^{-b} \tag{2.1}$$

where b is the negative slope of the log-log relationship of CSR and the number of cycles to liquefaction $(N_{\gamma=3.75\%})$. A depiction of this relationship is shown in Figure 2.8 (Ulmer et al., 2019). As seen in this Figure, a higher relative density (D_r) specimen exhibits a higher cyclic resistance ratio as the number of cycles required to reach liquefaction increases. Additonally, $N_{\gamma=3.75\%}$ decreases with increasing CSR values. The CRR that triggers liquefaction at 15 cycles can also be directly estimated from this relationship.

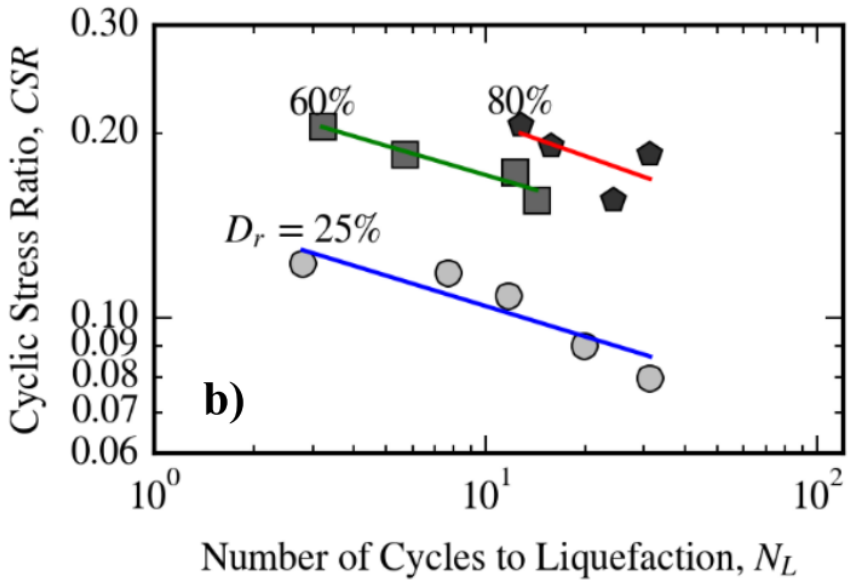

FIGURE 2.8: Cyclic resistance ratio (CRR) defined as single-amplitude shear strain γ =3.75%, $with\sigma_{vc}$ = 100kPa (Ulmer et al., 2019).

Verma et al., 2015 found the CRR to be decreasing with increasing initial static shear bias as shown in Figure 2.9.

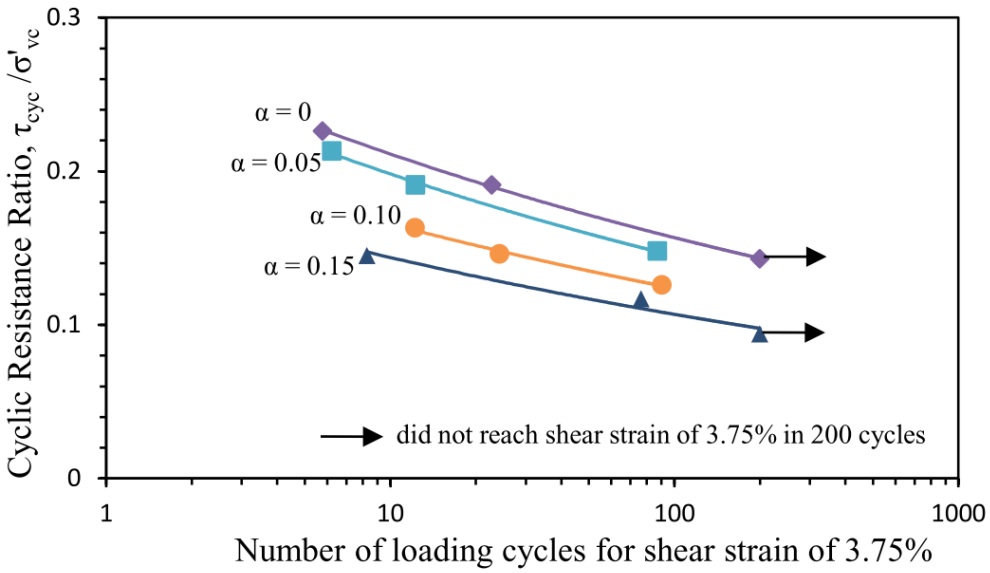

FIGURE 2.9: Effect of the initial static shear bias on the cyclic resistance ratio (CRR)(Verma et al., 2015).

2.5 Drained shear stress bias

The application of initial static shear stress (τ_{ff}) prior to cyclic loading influences the shear resistance. This shear stress is applied to mimic sloping ground conditions in the field or a horizontal ground loaded by a structure (Ingabire, 2019. The ratio between the static shear stress and the vertical effective stress is denoted with α and is expressed as

$$\alpha = \tau_{\alpha}/\sigma'_{vc} \tag{2.2}$$

This ratio is also known as initial static shear stress bias (Sanin, 2010) or pre-shear stress.

Verma et al., 2015 performed CV-CDSS tests under constant CSR values and varying α values, under a cyclic shear load frequency of 0.1 Hz. Their results showed that excess pore pressure and accumulation of shear strain increased with the initial static shear stress bias. Under cyclic loading, reconstituted silt specimens exhibited and increase in shear stiffness degradation with increasing loading cycles (Sanin, 2010).

2.6 Research Gap

As discussed in this chapter, many studies have been conducted to analyse the behaviour of sands and silts under seismic loading to induce liquefaction under undrained conditions. In this manner, the corresponding responses of the material in terms of cyclic shear stress and strain, and void ratio have been analysed. These tests are mainly performed using CDSS tests as these these tests are capable of measuring excess pore pressure within a sample. However, the use of direct shear test to study the liquefaction behaviour is not used as this type of test is incapable of measuring pore water pressures. The Geo-engineering lab has recently acquired a state of the art direct shear apparatus, manufactured by de Wille Geotechnik, capable of conducting cyclic direct shear test under various frequencies. The aim of this thesis is thus exploring the capabilities of this apparatus to perform stress-controlled cyclic direct shear tests to study the liquefaction response of fine-sand tailings under partially drained conditions. By performing the cyclic direct shear tests under constant vertical stress

and a certain frequency, the aim is to simulate these partially drained conditions. Thus, a series of laboratory tests will be performed to study the liquefaction response of the tailings under various initial void ratio's and relative density.
Following the literature review, the research gap and the round-robin program, the main research question of this thesis is formulated as follows:

"How useful is the cyclic direct shear test to study the liquefaction response of fine-sand tailings?"

To help answer this question the following sub questions are formulated:

1. **What is the influence of relative density to reach liquefaction criteria of γ = 3.75% under cyclic direct shear loading?**

   As evident from the literature review, the influence of relative density effects the cyclic resistance ratio the soils. However, these tests are conducted using direct simple shear under undrained conditions. There is limited data on the influences of relative density in a cyclic direct shear test which can also simulate partially drained conditions.

2. **How does the drained shear bias influence the cyclic shear response in cyclic direct shear tests and how does it compare between dense and loose samples?**

   The application of the drained shear bias helps study liquefaction of soils under sloping ground conditions. By performing tests where the drained shear bias is applied and where level ground conditions is assumed (no shear bias application), the effect on the cyclic shear response can be investigated in a partially drained environment.

3. **How does the fine sand tailings respond when subjected to post-cyclic loading?**

   Post-cyclic shear tests in the literature have been mainly performed on tests which underwent cyclic shearing under constant-volume conditions. By performing post-cyclic shear tests, the influence of CSR and the constant stress conditions can be investigated and the residual shear strength can be determined.

Chapter 3

Methodology

3.1 Material properties

The fine-sand that is used in the experiments, originate from mine tailings and have been acquired from the University of Western Australia. Relevant laboratory tests are conducted to determine the necessary material properties. The specific gravity (G_s) is determined following the ASTMD555014, 2014 standard, and the minimum void ratio (e_{min}) and the maximum void ratio (e_{max}) are determined according to ASTMD4254, 2016 and ASTMD4253, 2016, respectively. The properties of the material are summarised in 3.1. The grain size distribution of the material is not determined in the laboratory as this property was provided for by the supplier. The as received water content is determined to be 6.2%.

TABLE 3.1: Fine-sand tailings properties.

Material property		**Standard**
e_{max}	1.53	ASTM D4253
e_{min}	0.54	ASTM D4254
G_s	2.82	ASTM D5550
Grain size	55%<75um 39%<38um 6%>75um	Acquired
water content	6.2%	

3.2 Sample Preparation Procedure

The samples are prepared using the Moist Tamping (MT) technique, using the under-compaction method, as proposed by Ladd et al., 1978. The MT technique incorporates a tamping method, where the specimen is assembled in layers. Under-compaction refers to the fact that each layer is compacted to a lower relative density than the target relative density. The difference between these densities is defined as percent under-compaction(U_n). The U_n value should vary linearly from the bottom to the top layer, with the bottom layer having the largest U_n value and the top layer is typically zero. The goal of this method is to make a sample with a relatively uniform void ratio throughout the specimen's height. A multi-layer (ML) method is developed by Jiang et al., 2003 based on the under-compaction principle of Ladd et al., 1978. The required height of the sub layers using the ML method is determined through Equation 3.1:

$$h_n = \frac{h_t}{n_t} \cdot n \tag{3.1}$$

where, h_t is the final height of the sample, n_t is the total number of layers, n is the n^{th} layer, and h_n is the height of the n^{th} sample.

The samples are prepared following the ML method in equal weight and equal height. To start the sample preparation, first the dimensions of the mould is measured. The tests are conducted with a square shear box, with a side of 100 mm. The shear box and the rest of its parts are shown in Figure 3.1.

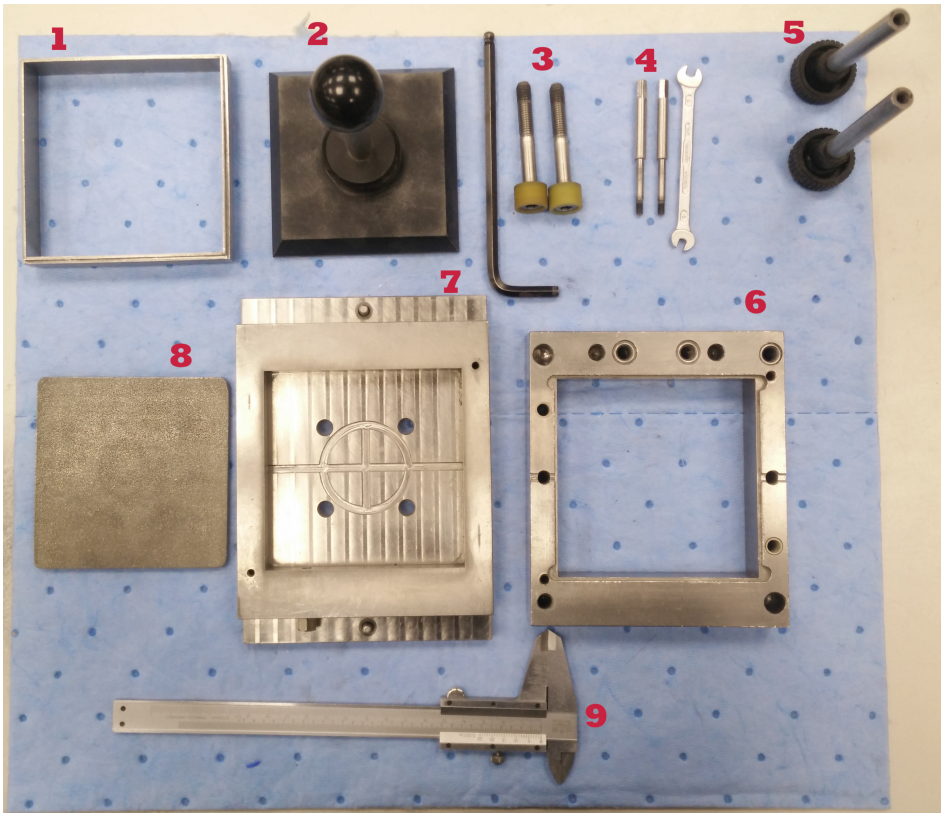

FIGURE 3.1: The shear box components. 1. Extension placed on the top of the shear box for the sample preparation, 2. Tamper tool , 3. Screws to secure the top platen on the top of the shear box, 4. Pins to screw the upper and lower halves of the shear box, 5. Handles of the shear box, 6. Top half of the shear box, 7. Bottom half of the shear box, 8. Porous stone, 9. Caliper.

The shear box is assembled by first screwing the top and bottom halves with the pins and placing the porous and the bottom of the shear box. The handles are tightened at either side of the shear box for easier lifting and moving the assembly. To prepare the sample, the material should be mixed with water to achieve a specimen with known water content. Ladd et al., 1978, Frost et al., 2003, and Amini et al., 2000 deemed a water content of 5-7% sufficient for the sand sample preparation. Hence the samples for this study are prepared using the as received water content of the material. The tests are performed on dense and loose prepared samples. The dense samples are prepared and initial target relative density of 65% and the loose samples are prepared with an initial target relative density of 20%. The values for the relative density is determined based on the available tailings material and the number of tests aimed to be performed. The required dry weight (M_d) and the total weight (M_t) for each sample is given in Table 3.2. The target void ratio (e_0) for the dense and loose samples are 0.89 and 1.33, respectively.

The dense samples are prepared in five layers of equal weight and height using the ML method. The loose samples are prepared in seven layers of equal weight and equal height. A sketch of these layered samples is shown in Figure 3.2. The moist weight required for each layer is determined by Equation 3.2

$$W_L = W_T / n_t \tag{3.2}$$

TABLE 3.2: Sample weights.

D_r	e_0	V_s [cm^3]	M_d [gr]	water content (6.2%) [gr]	M_t [gr]
65%	0.89	105.82	298.4	18.50	316.90
20%	1.33	85.76	241.85	15.0	256.85

where W_T is the total wet weight and n_t the total number of layers.

FIGURE 3.2: Multi-layered sample preparation sketch of A. dense samples, and B. loose samples.

Each layer is sequentially placed into the shear box. Starting from the first layer, the required amount is weighed and carefully spooned into the shear box and lightly tapped until the desired height of the layer is reached. The top of this layer is then scarified before the next layer is placed to ensure a more uniform connection between each layer (Salamatpoor et al., 2014). This process is repeated until all the layers are placed. The procedure further depicted in Appendix A.

The void ratio of each layer can also be determined through Equation 3.3, as suggested by Jiang et al., 2003.

$$e_n = \bar{e} + (\bar{e} + 1)\frac{U_n}{100 \cdot n} \tag{3.3}$$

where $\bar{e}$ is the desired void ratio of the whole specimen.

3.3 Laboratory testing procedure

Stress-controlled cyclic direct shear (SC-CDS) tests will be carried out in a 10 cm x 10 cm shear box on the direct shear loading apparatus, manufactured Wille Geotechnik, shown in Figure 3.3. The specimens will be prepared using the MT method. The shear box apparatus is controlled using the GEOsys Creator software.

After the software is initialised, the shear box is securely placed in the chamber. The chamber is then filled with water to create a water bath around the shear box and submerge the sample within. After visually observing that the sample is saturated, the top platen, attached to the load piston, is lowered just before that top platen makes contact with the sample. The contact with the sample is established using a different shear test license. A contact stress of 1 kPa is applied using this license to ensure that there is no gap between the top platen

and the sample. A small contact stress is chosen to minimise major settlements in the sample. After the contact stress is established, the license is switched to the stress-control license program from where the consolidation stage is initiated. The test run parameters for the SCCDS test are shown in Figure 3.4.

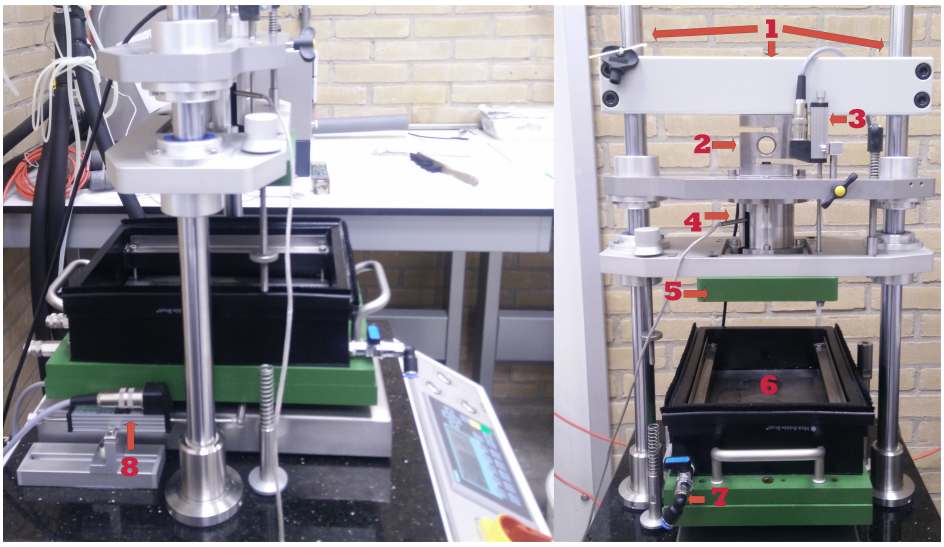

FIGURE 3.3: Direct shear loading system. 1. Loading frame, 2. load cell, 3. vertical displacement transducer, 4. loading piston. 5. top platen, 6. shear box chamber, 7. drainage outlet, 8. horizontal displacement transducer.

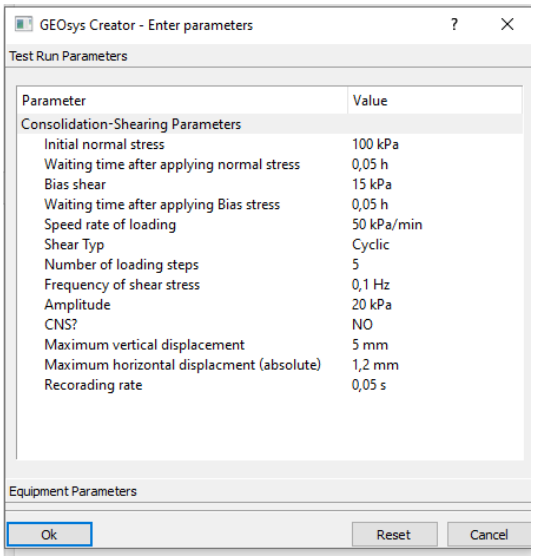

FIGURE 3.4: Consolidation and shearing input parameters for the SCCDS tests.

3.3.1 Consolidation phase

The next stage in the testing procedure is the consolidation stage of the sample. A vertical effective stress of 200 kPa is applied at a loading rate of 5 kPa/min for the dense samples and 0.5 kPa/min for the loose samples. A lower loading rate is applied to the loose samples to minimise any rapid settlements from occurring due to their higher void ratio. After the vertical effective stress is established, the samples are kept under this stress for 3 hours. This gives the samples sufficient time to consolidate and attain unchanging vertical deformation.

3.3.2 Drained static shear bias application phase

After the end of the consolidation waiting time, the sample subjected to a drained shear bias (τ_α) of 30 kPa, which is applied at a shear loading rate of 0.1 kPa/min. A low rate of loading is chosen to make sure that excess pore water pressure are quickly dissipated. After the drained shear bias is applied, a waiting time of 1 hour is set to ensure that any excess pore water pressure has sufficient time to dissipate and that the horizontal and vertical strains can stabilize.

3.3.3 Cyclic shear loading phase

After the waiting time of the previous phase, the cyclic direct shear test is automatically started. Stress-controlled cyclic shear load is applied in the form of a sinusoidal wave with a frequency of 0.1 Hz and a fixed shear amplitude. The test will conclude when the maximum horizontal shear displacement is reached or when the set number of cycles (given as "Number of loading steps" in Figure 3.4) is reached.

3.3.4 Post-cyclic shear test phase

After the cyclic shear test, a post-cyclic shear test is performed on the samples to assess any residual shear strength in the samples. For this test the samples are reconsolidated to the initial consolidation stress of 200 kPa. The tests start with the shear box in its neutral position (zero shear displacement) under strain-controlled and constant vertical load conditions. The test is concluded when the set shear displacement is reached.

3.4 Test program

The SC-CDS test is split into three test programs with varying conditions. A summary of the test program is presented in Table 3.3. These three test programs have been issued by UWA for the round robin. *Program A* consists of a set of six tests performed on loose samples ($D_r = 20\%$, $e = 1.33$) with τ_α of 30 kPa and varying CSR values. *Program B* consists of a set of six tests performed on dense samples ($D_r = 65\%$, $e = 0.89$) and τ_α of 30 kPa. The samples from *Program C* are similar to the samples of Program A, consisting of a set of five loose samples. The only difference is that no τ_α is applied on these samples prior to the cyclic shearing phase. The proposed CSR values in the table is decided by the author by performing the cyclic direct shear tests with various CSR's. Tests with the best responses have then been selected for each program. A sketch of these test procedures is depicted in Figure 3.5. Two monotonic tests are additionally performed on dense samples under strain-controlled conditions to determine the strength parameters of the fine-sand tailings.

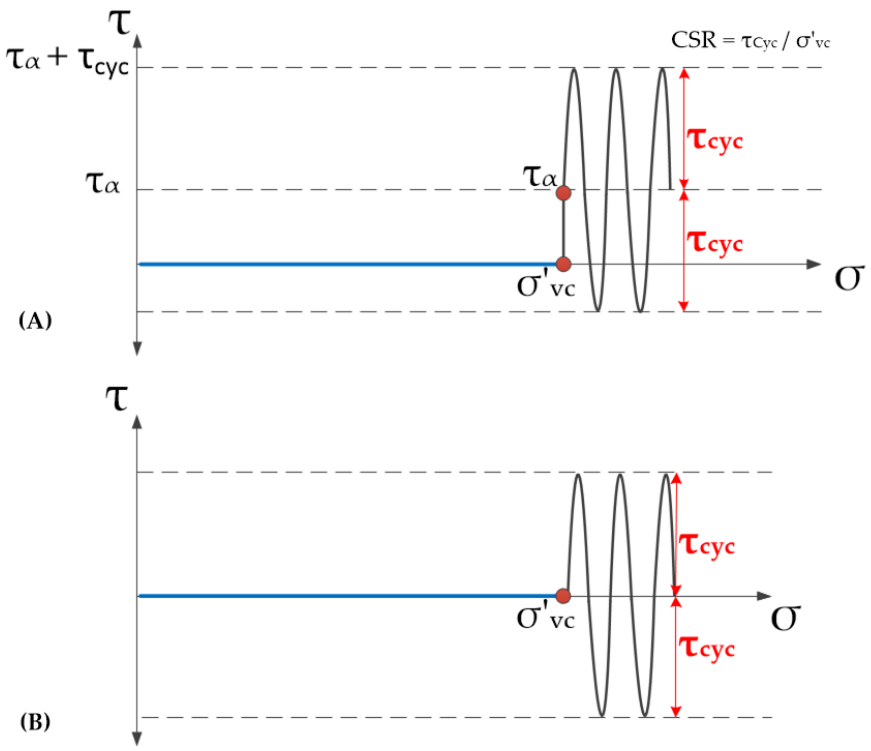

FIGURE 3.5: (A) Sketch of the cyclic direct shear test procedure for programs A and B with applied drained shear bias. (B) depicts the sketch of the test procedure of program C.

3.5 Test limitations

The aim of this thesis is to investigate to what extent a shear box can be used to study the cyclic response of fine-sand tailings. However, to test the tailings for its liquefaction criteria comes with some limiting factors that should be taken into account.

- It is not possible to measure any excess pore water pressure generation in the shear box test
- The liquefaction criteria is only known in terms of shear strain (γ), which is expressed as horizontal deformation over initial sample height. As the SC-CDS test only records the horizontal displacement and no horizontal deformation, it is not possible to accurately determine the shear strain.

Finally, the direct shear loading apparatus is optimised for strain-controlled testing, therefore the stress-controlled testing license comes with some drawbacks. The cyclic frequency input is not fully utilised during the tests, mainly when cycle reaches close to the target shear amplitude, the loading rate appears to slows down drastically, resulting in a longer cycle time than intended.

TABLE 3.3: Test program.

			Initial state		Consolidated state					
	Test#	Test ID	e_i [-]	Dr_i [%]	e_c [-]	Dr_c [%]	τ_α[kPa]	τ_{cyc}/σ'_{vc} (CSR)	τ_{cyc} [kPa]	$N_{\gamma=3.75\%}$
Program A	1	LSRD-200-A1	1.33	20			30	0.125	25	
	2	LSRD-200-A2						0.135	27	
	3	LSRD-200-A3						0.15	30	
Loose samples	4	LSRD-200-A4						0.16	32	
	5	LSRD-200-A5						0.175	35	
	6	LSRD-200-A6						0.2	40	
Program B	1	DSRD-200-B1	0.89	65			30	0.15	30	
	2	DSRD-200-B2						0.16	32	
	3	DSRD-200-B3						0.175	35	
Dense samples	4	DSRD-200-B4						0.185	37	
	5	DSRD-200-B5						0.2	40	
	6	DSRD-200-B6						0.225	45	
Program C	1	LSR-200-C1	1.33	20			-	0.2	40	
	2	LSR-200-C2						0.21	42	
	3	LSR-200-C3						0.215	43	
Loose samples	4	LSR-200-C4						0.225	45	
	5	LSR-200-C5						0.25	50	

Chapter 4

Results

The main objective of this thesis is to investigate how useful Stress-controlled cyclic direct shear test can be to study the liquefaction behaviour of fine-sand tailings. In chapter 3, the methodology and the test procedure are explained. Following this procedure, three test programs are made. The test results of these programs are presented in this chapter, where each test phase is separately looked at. Furthermore, post-cyclic shear tests are performed on some test samples to determine their post-cyclic shear stress.

4.1 Monotonic testing

The main purpose of the monotonic tests was to determine the friction angle (ϕ') and the cohesion (c') of the tailings. Two tests were performed on dense samples with initial relative density of 65% and were consolidated at vertical effective stresses of 100 kPa and 200 kPa. Both tests were performed strain-controlled under constant normal load conditions. The samples were sheared with a displacement rate of 0.1 mm/min until a maximum shear displacement of 10 mm was reached. The results of the monotonic tests are depicted in Figure 4.1. Figure 4.2 depicts the range of volume change behaviour from dilation (negative vertical displacement) to contraction (positive vertical displacement). It is observed that the samples dilated at the start of shearing and then contracted until the end of the test. The maximum shear stress, τ_{max}, reached by both tests were plotted against their respective vertical effective stress, σ_v, to form the Mohr-Coulomb (MC) failure line, as shown in Figure 4.3. From this failure line, the strength parameters of the fine-sand tailings is determined. The friction angle, ϕ', is calculated to be 33.8° and the cohesion, c', is found to be 0 kPa.

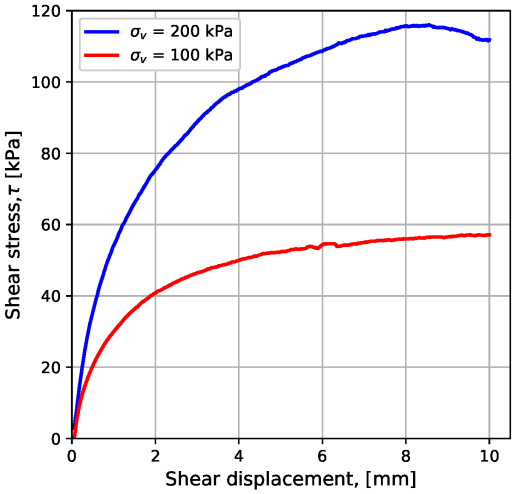

FIGURE 4.1: Mohr-Coulomb failure line of the monotonic shear tests.

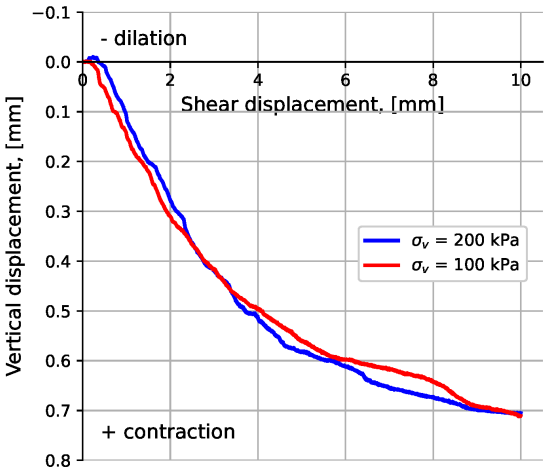

FIGURE 4.2: Vertical displacement versus shear displacement.

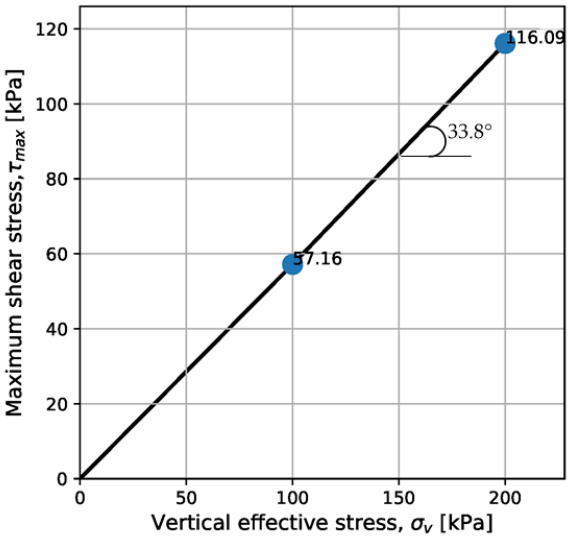

FIGURE 4.3: Mohr-Coulomb failure line of the monotonic shear tests.

4.2 Cyclic direct shear response of fine-sand tailings

This section presents the cyclic shear responses of the three test programs. First, the results of the consolidation stage is analysed followed by the shear response during the drained shear bias application. After that, the cyclic shear responses are illustrated, and lastly, the results of the post-cyclic shear tests are shown.

4.2.1 Consolidation stage

In Figure 4.4, the change in void ratio (e) during the consolidation phase is shown of the loose samples tested in program A. The behaviour of these loose samples during the consolidation stage is more or less the same, except for sample LSRD-200-A2, which appears to be consolidating much faster compared to the other tests, despite having the same loading rate.

A possible reason for this could lie in some variations which might have occurred during the sample preparation process when the samples are compacted in layers. Another reason can be that there were some air bubbles still present after saturating the sample, which can escape during consolidation and thus compressing the sample much faster compared to the other samples.

Figure 4.5 depicts the change in void ratio of the tests conducted in program B. The tests in this program exhibit similar behaviour during the consolidation stage. A similar consolidation response as LSRD-200-A2 is observed in test DSRD-200-B5, where this sample consolidates faster than the others. The same argument mentioned for LSRD-200-A2 can be made here.

Figure 4.6 depicts the consolidation stage of program C. All samples in this program reached similar end of consolidation void ratio, and the trend observed in the Figure is also identical to each other.

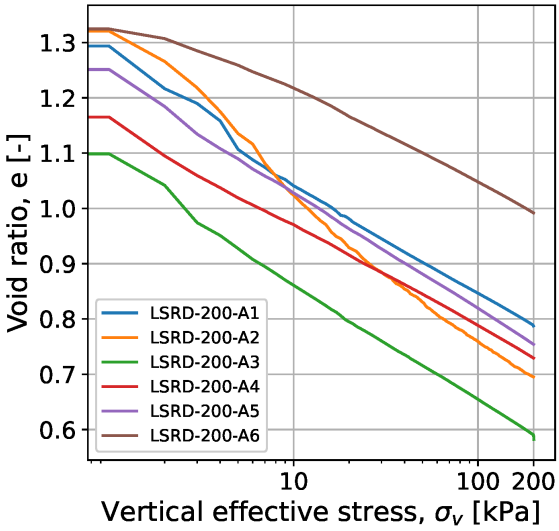

FIGURE 4.4: Change in void ratio of loose samples from program A at the consolidation stage.

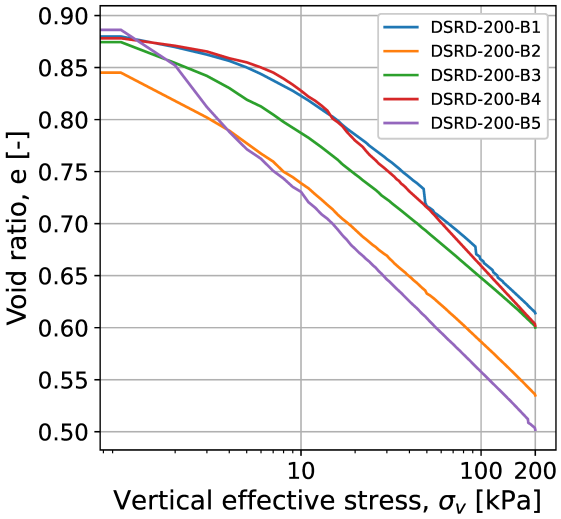

FIGURE 4.5: Change in void ratio of dense samples from program B at the consolidation stage.

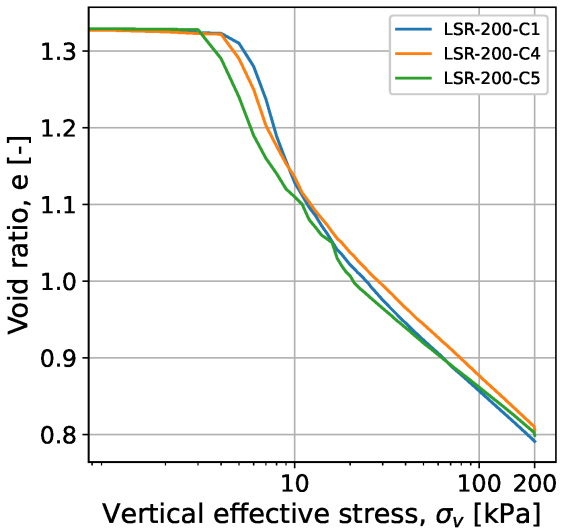

FIGURE 4.6: Change in void ratio of loose samples from program C at the consolidation stage.

A tabulated overview of the consolidation stage is given in Table 4.1. From this table it is observed that the consolidated void ratio within each program lie fairly close to each other, with the largest variations observed in program A.

TABLE 4.1: Change in void ratio (e) and relative density (Dr) at the end of consolidation stage.

	Test#	Test ID	e_i [-]	Dr [%]	e_c [-]	Dr_c [%]	e_{mean}	Standard Error (SE)
Program A	1	LSRD-200-A1			0.78	75.8		
	2	LSRD-200-A2			0.69	84.8		
	3	LSRD-200-A3	1.33	20	0.58	96.0	0.75	0.055
Loose samples	4	LSRD-200-A4			0.72	81.8		
	5	LSRD-200-A5			0.75	78.8		
	6	LSRD-200-A6			0.99	54.5		
Program B	1	DSRD-200-B1			0.53	101.0		
	2	DSRD-200-B2			0.53	101.0		
	3	DSRD-200-B3	0.89	65	0.59	94.9	0.56	0.016
Dense samples	4	DSRD-200-B4			0.6	93.9		
	5	DSRD-200-B5			0.5	104.0		
	6	DSRD-200-B6			0.58	96.0		
Program C	1	LSR-200-C1			0.79	74.7		
	2	LSR-200-C2			0.82	71.7		
Loose samples	3	LSR-200-C3	1.33	20	0.89	64.6	0.82	0.018
	4	LSR-200-C4			0.81	72.7		
	5	LSR-200-C5			0.8	73.7		

4.2.2 Drained shear bias

The drained shear bias (τ_α) is a pre-shear stress applied after the consolidation stage and before the start of the cyclic stage. This stress is applied to simulate sloping ground conditions in shear tests. A shear bias (α) of 0.15 is used which is equivalent to 30 kPa shear stress. This stage is only applied to the tests in program A and program B. The responses of this stage are presented in Figure 4.7 for program A and in Figure 4.9 for program B. When comparing the shear responses, it is apparent that the loose samples of program A reached a larger shear displacement than the dense samples from program B. The volume changes observed in Figure 4.8 appears to follow the expected response of contraction (positive

vertical displacement), whereas Figure 4.10, depicting the volume changes of program B, show small amounts of dilation, followed by significant contractive behaviour. However, this dilation is too small and can occur by the fluctuation of the shear displacement due to stress-controlled shearing. The samples from program A also appear to contract more than those of program B.

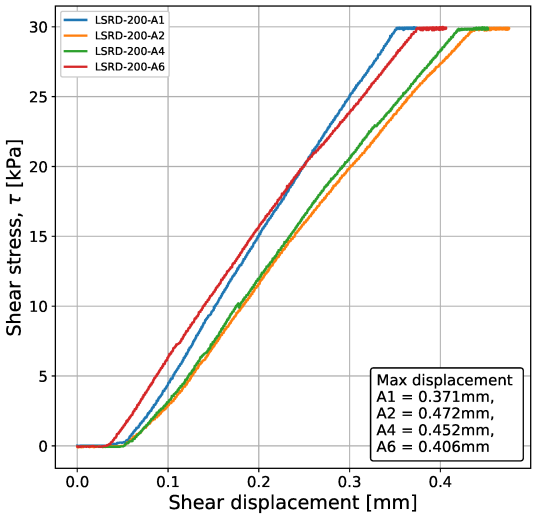

FIGURE 4.7: Drained shear bias response of program A.

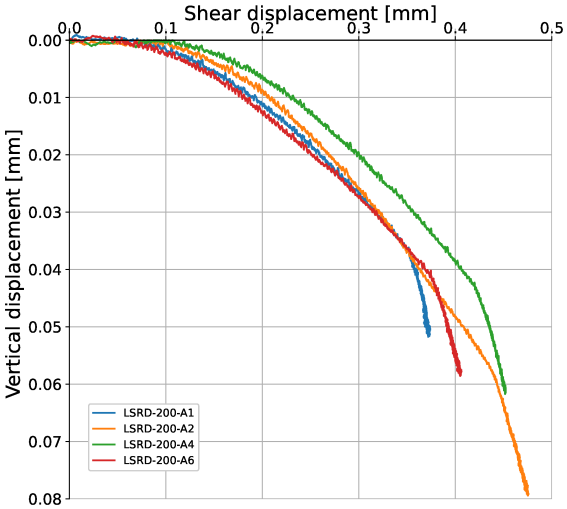

FIGURE 4.8: Vertical displacement vs. horizontal displacement of program A.

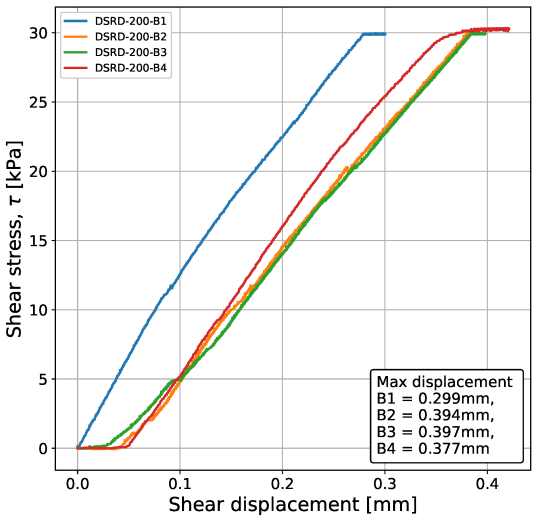

FIGURE 4.9: Drained shear bias response of program B.

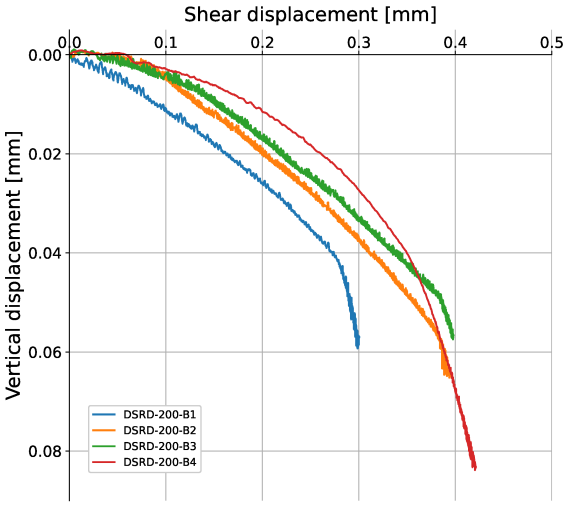

FIGURE 4.10: Vertical displacement vs. horizontal displacement of program B.

4.2.3 Cyclic direct shear response

A full overview of the cyclic shear responses is given in Table 4.2. As evident from the table, some tests reached the liquefaction criteria of 3.75% shear strain in the same number of cycles ($N_{\gamma=3.75\%}$). Hence, only tests with differing $N_{\gamma=3.75\%}$ will be further analysed. The

TABLE 4.2: Overview of the cyclic shear responses.

	Test#	Test ID	CSR τ_{cyc}/σ'_{vc}	τ_{cyc} [kPa]	$N_{\gamma=3.75\%}$	γ_{max} [%]
Program A	1	LSRD-200-A1	0.125	25	>200	2.93
	2	LSRD-200-A2	0.135	27	36	4.09
	3	LSRD-200-A3	0.15	30	4	5.05
Loose samples	4	LSRD-200-A4	0.16	32	4	5.26
	5	LSRD-200-A5	0.175	35	4	5.08
	6	LSRD-200-A6	0.2	40	1	5.44
Program B	1	DSRD-200-B1	0.15	30	47	4.11
	2	DSRD-200-B2	0.16	32	19	4.77
	3	DSRD-200-B3	0.175	35	15	4.71
Dense samples	4	DSRD-200-B4	0.185	37	1	6.11
	5	DSRD-200-B5	0.2	40	1	5.28
	6	DSRD-200-B6	0.225	45	1	6.82
Program C	1	LSR-200-C1	0.2	40	>200	2.46
	2	LSR-200-C2	0.21	42	>200	3.5
	3	LSR-200-C3	0.215	43	>200	3.45
Loose samples	4	LSR-200-C4	0.225	45	8	4.05
	5	LSR-200-C5	0.25	50	1	3.9

remaining test results can be found in Appendix B. The number of cycles is determined by dividing the total test time by the time it took for the first cycle to complete.

Test results of SCCDS test response of program A

The samples in program A were prepared with a target D_r of 20% and the tests were performed with τ_α of 30 kPa. Figure 4.11 shows the cyclic shear response of test LSRD-200-A1 with a cyclic shear amplitude (τ_{cyc}) of 25 kPa. It is observed that even after 200 cycles the test did not reach the liquefaction criteria of γ = 3.75% and only reaching a maximum shear strain of 2.93%. Figure 4.11(a) shows the shear strain curve development against the cyclic shear stress, starting at τ_α = 30 kPa, and consistently varying between $\tau_\alpha + \tau_{cyc}$ and $\tau_\alpha - \tau_{cyc}$. Figure 4.11(b) depicts the vertical stress response during the cyclic test. A closer look at the data showed that the vertical stress decreased with an average of 4 kPa each time towards the shear direction $\tau_\alpha + \tau_{cyc}$ and regained its vertical stress in the opposite shear direction. Figure 4.11(c) shows the total shear strain development with increasing number of cycles. It is also observed that the cycles are getting closer to each other as time progresses, indicating that the time needed to complete a full cycle becomes less. The blue dotted line in this figure shows an increase in the minimum strain value, indicating the presence of plastic shear strain development. Figure 4.11(d) shows the consistent variation of the cyclic shear stress through time as recorded by the GEOsys creator software. Furthermore, Figures 4.11(a) and 4.11(d) showed consistent behaviour for all the tests performed and is therefore excluded from the remaining test results.

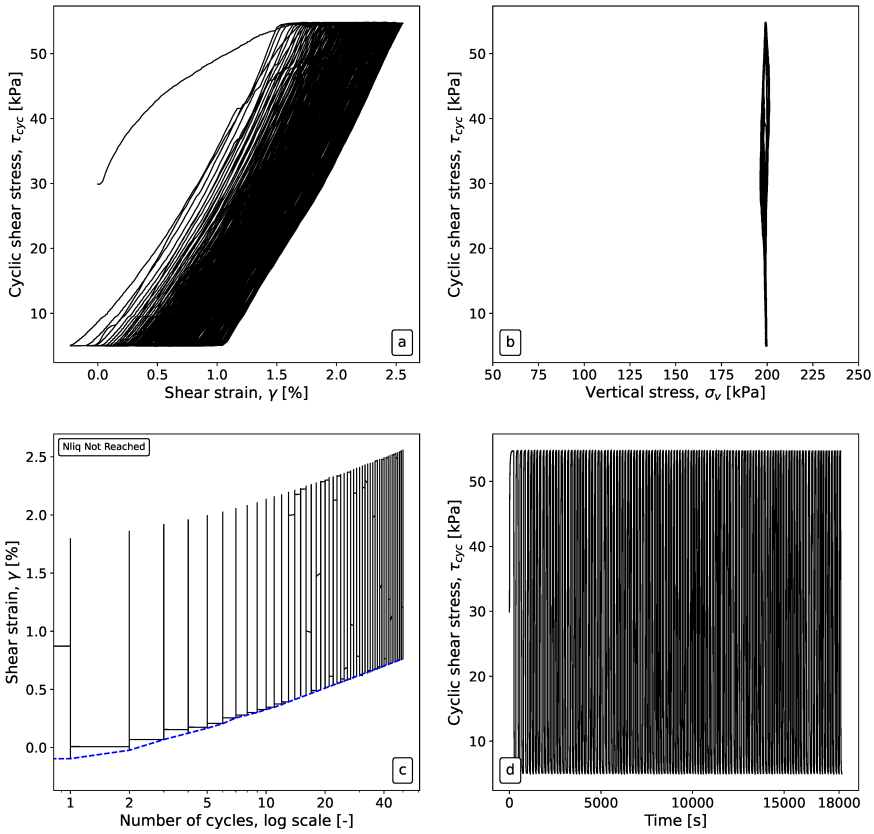

FIGURE 4.11: Test ID: LSRD-200-A1. SCCDS test performed on a loose sample using a cyclic shear amplitude of 25 kPa. a. Stress-strain response, b. Vertical stress behaviour against cyclic shear stress, c. shear strain development, d. Cyclic shear stress response against time.

Increasing the shear amplitude by 2 kPa (τ_{cyc} = 27 kPa) for test LSRD-200-A2, the test reached $N_{\gamma=3.75\%}$ in significantly less number of cycles, as seen in Figure 4.12(a). Test LSRD-200-A3 through A5 have all reached $N_{\gamma=3.75\%}$ within 4 cycles, as seen in Table 4.2. For further analysis of program A, test LSRD-200-A4 is chosen out of these three tests, the result of which is shown in Figure 4.13. Figure 4.14 shows that τ_{cyc} of 40 kPa is high enough to reach $N_{\gamma=3.75\%}$ within 1 cycle. Similar to Figure 4.11, all the tests in program A exhibited plastic shear strain development, denoted by the blue trend line.

Figures 4.12(b), 4.13(b) & 4.14(b) show the vertical stress responses of these tests. For all tests the average vertical stress remained around 200 kPa, with a slight decrease in τ_α + τ_{cyc} direction. The vertical stress fluctuated in all the tests varied between 193-202 kPa.

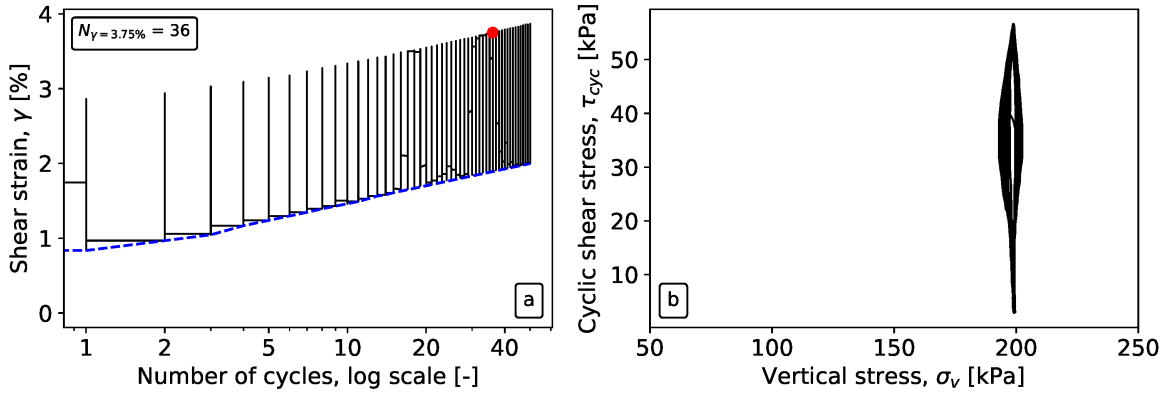

FIGURE 4.12: Test ID: LSRD-200-A2. SCCDS test performed on a loose sample using a cyclic shear amplitude of 27 kPa. a. shear strain development wrt. number of cycles, b. Vertical stress response against cyclic shear stress.

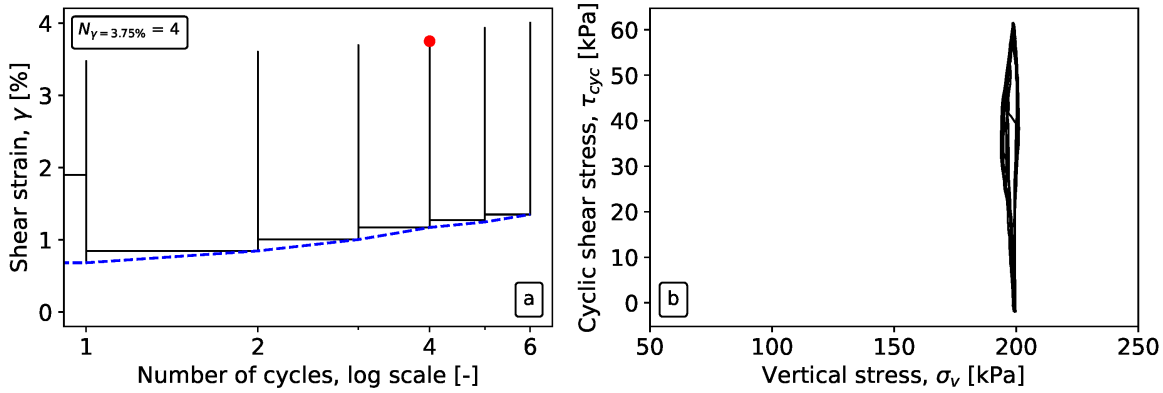

FIGURE 4.13: Test ID: LSRD-200-A4. SCCDS test performed on a loose sample using a cyclic shear amplitude of 32 kPa. a. shear strain development wrt. number of cycles, b. Vertical stress behaviour against cyclic shear stress.

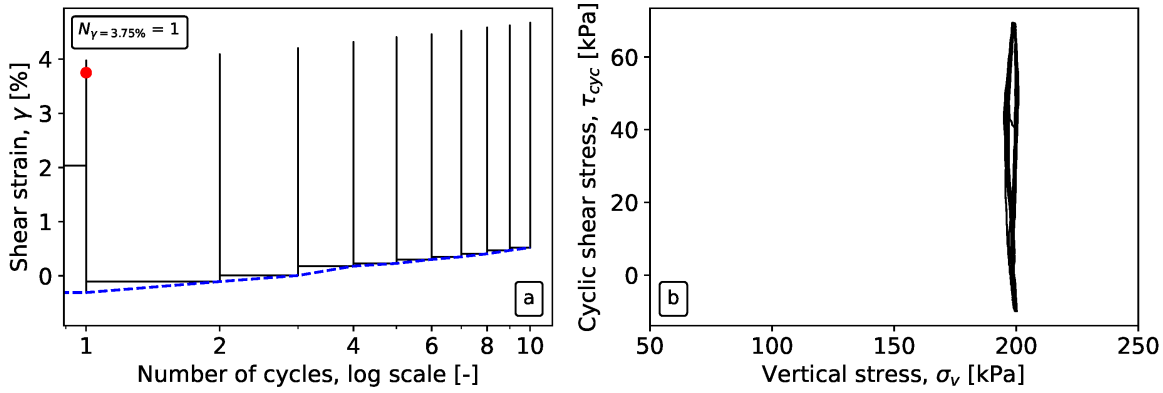

FIGURE 4.14: Test ID: LSRD-200-A6. SCCDS test performed on a loose sample using a cyclic shear amplitude of 40 kPa. a. shear strain development wrt. to number of cycles, b. Vertical stress behaviour against cyclic shear stress.

The relationship of the vertical -and shear displacement is shown in Figure 4.15. The vertical displacement indicates the change in height during the cyclic test, where a positive value indicates the sample is contracting. It is evident from this figure that during the initial

cycles the sample undergoes large amounts of contraction then gradually decreases. It can also be noted that the application of higher τ_{cyc} resulted in higher vertical displacement at the beginning. This is clearly seen in the response for LSRD-200-A6 where the test was performed with fewer cycles but undergoing the largest vertical displacement.

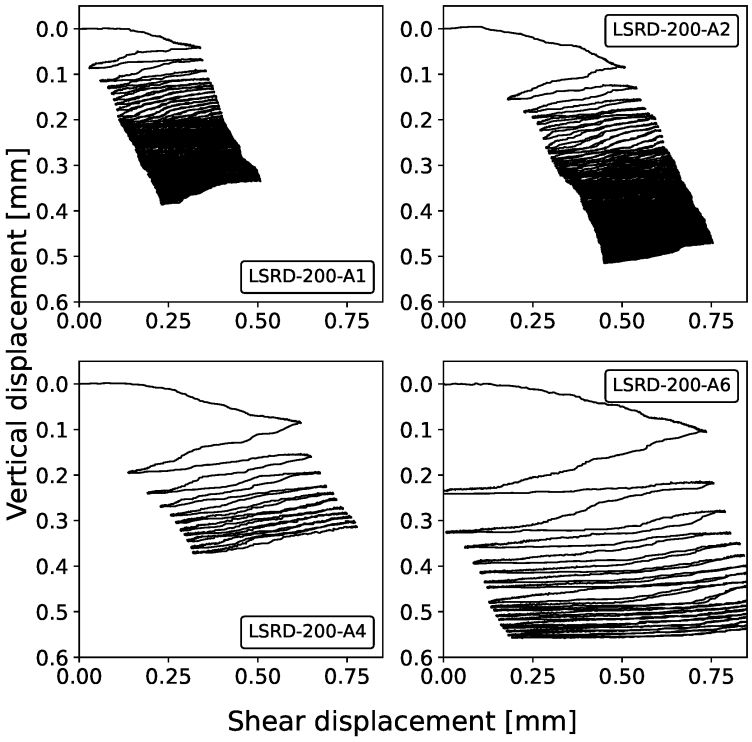

FIGURE 4.15: Response of the vertical extension with respect to the shear extension of the discussed tests.

Test results of SCCDS test response of program B

Program B consists of tests performed on dense (Dr = 65%) samples and τ_{α} of 30 kPa. These samples required a slightly higher τ_{cyc} to reach $N_{\gamma=3.75\%}$, compared to program A. Figures 4.16(a), 4.17(a), 4.18(a) & 4.19(a) presents the shear strain response against the number of cycles. It shows the expected result that higher τ_{cyc} implementation required less cycles to reach $N_{\gamma=3.75\%}$. Compared to the loose samples, the dense samples needed a lower τ_{cyc} to reach $N_{\gamma=3.75\%}$ in 1 cycle. Similar to program A, the samples in Program B also exhibit plastic strain development in the cyclic stage, as illustrated with the blue dotted line in the figures.

Figures 4.16(b), 4.17(b), 4.18(b) & 4.19(b) depicts the vertical stress responses of these tests. It is noticed that similar to program A, the vertical stress for the dense samples also fluctuated during the cyclic stage. Also noticeable is that for test DSRD-200-B1 the stress decrease occurred the most in the τ_{α} - τ_{cyc} direction. The the vertical stress fluctuated within a range of 192-202 kPa for the tests on the dense samples, which is similar to the response observed for the loose samples.

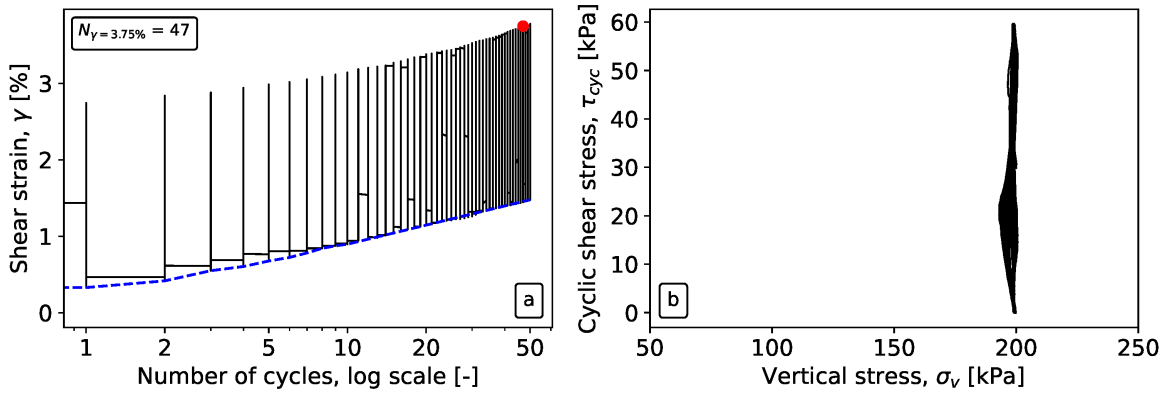

FIGURE 4.16: Test ID: DSRD-200-B1. SCCDS test performed on a dense sample using a cyclic shear amplitude of 30 kPa. a. shear strain development wrt. number of cycles, b. Vertical stress response against cyclic shear stress.

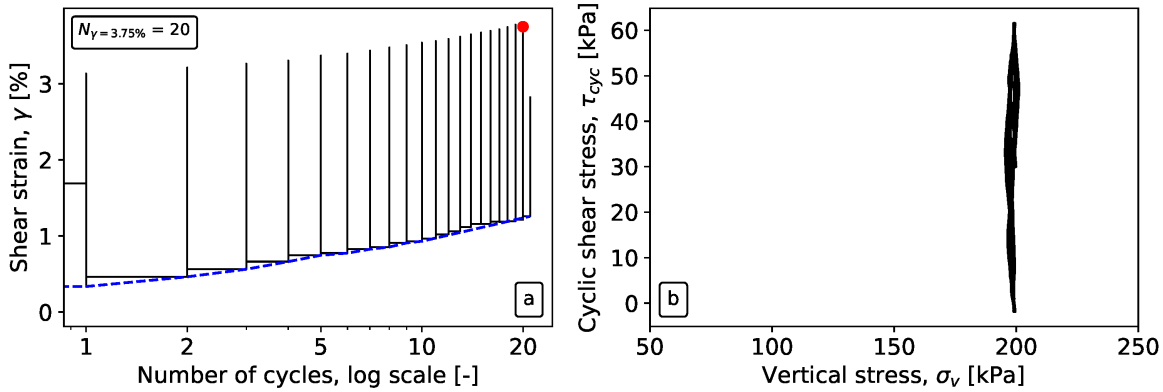

FIGURE 4.17: Test ID: DSRD-200-B2. SCCDS test performed on a dense sample using a cyclic shear amplitude of 32 kPa. a. shear strain development wrt. number of cycles, b. Vertical stress response against cyclic shear stress.

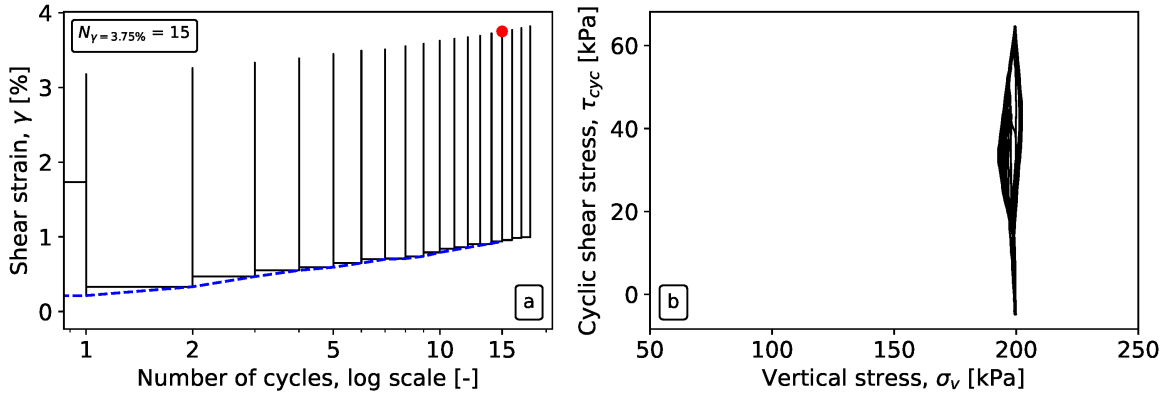

FIGURE 4.18: Test ID: DSRD-200-B3. SCCDS test performed on a dense sample using a cyclic shear amplitude of 35 kPa. a. shear strain development wrt. number of cycles, b. Vertical stress response against cyclic shear stress.

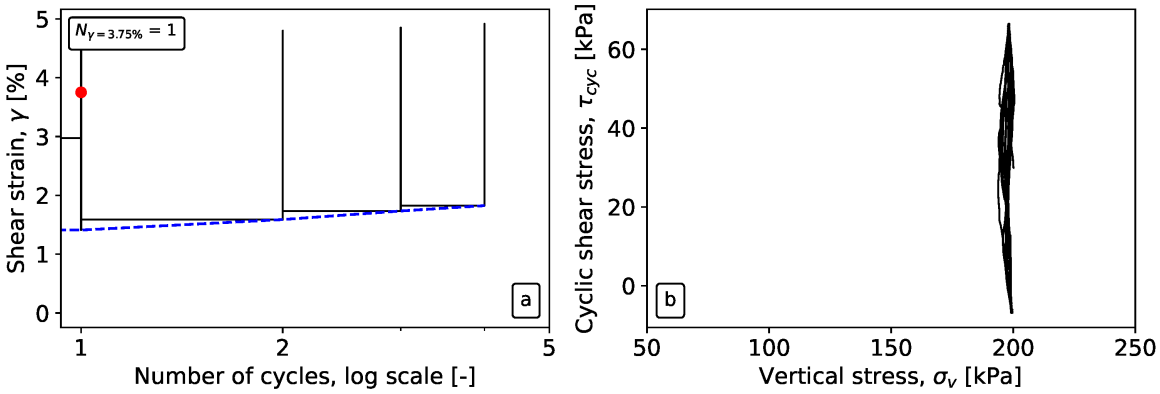

FIGURE 4.19: Test ID: DSRD-200-B4. SCCDS test performed on a dense sample using a cyclic shear amplitude of 37 kPa. a. shear strain development wrt. number of cycles, b. Vertical stress response against cyclic shear stress.

Figure 4.20 depicts the change in vertical displacement against the shear displacement. The dense samples show a higher degree of contraction as opposed to the loose samples from program A.

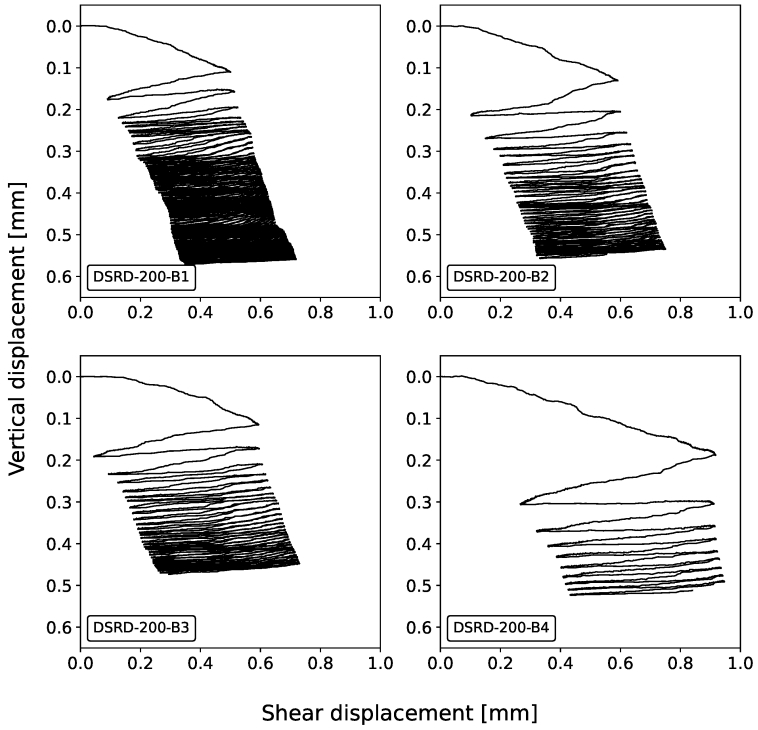

FIGURE 4.20: Response of the vertical extension with respect to the shear extension of the discussed tests.

Test results of SCCDS test response of program C

The tests in program C were performed on loose (Dr = 20%) samples with no drained shear bias application, thus starting the cyclic shearing from the 'zero strain' position of the shear box. For these tests a much higher τ_{cyc} was needed to achieve $N_{\gamma=3.75\%}$. Table 4.2 shows that τ_{cyc} of 40 kPa through 43 kPa for tests LSR-200-C1, C2 & C3, respectively did not reach $N_{\gamma=3.75\%}$ even after the maximum allowed cycles by the direct shear apparatus. A part of the shear strain response of LSR-200-C1 is extracted to show the response of this sample

in Figure 4.21(a). Increasing τ_{cyc} to 45 kPa for test LSR-200-C4 showed that $N_{\gamma=3.75\%}$ was reached in 8 cycles, as shown in Figure 4.22(a) and for τ_{cyc} of 50 kPa, applied on test LSR-200-C5, within one cycle as depicted in Figure 4.23(a). Furthermore, the tests developed far less plastic strains, compared to the previous test programs. Test LSR-200-C1 developed a total of 0.21% plastic strain during the whole cyclic stage. In LSR-200-C4 a change of 0.82% strain in 8 cycles is observed, whereas LSR-200-C5 developed 0.5% strain in just 3 cycles. This indicates that with the application of higher shear amplitudes on the samples of program C, larger plastic strains are developed in lower number of cycles It is also interesting to note that the vertical stress fluctuations of these tests are also much higher, as seen in Figures 4.21(b), 4.22(b) & 4.23(b). Additionally, the vertical stresses tended to decrease in $+\tau_{cyc}$ direction, similar to programs A and C.

Figure 4.24 shows the relationship of the shear- and vertical displacements for the tests discussed here. A higher vertical extension is observed for these tests compared to programs A, which also consisted of loose samples.

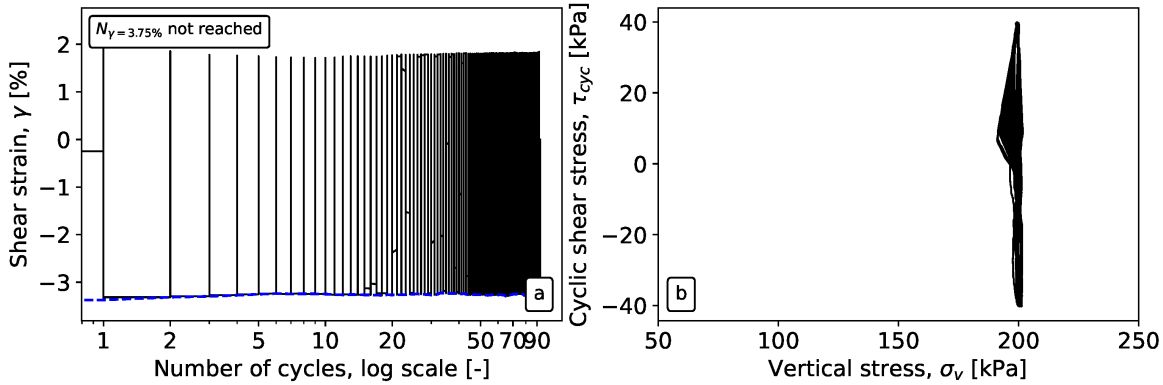

FIGURE 4.21: Test ID: LSR-200-C1. SCCDS test performed on a loose sample using a cyclic shear amplitude of 40 kPa. a. shear strain development wrt. number of cycles, b. Vertical stress response against cyclic shear stress.

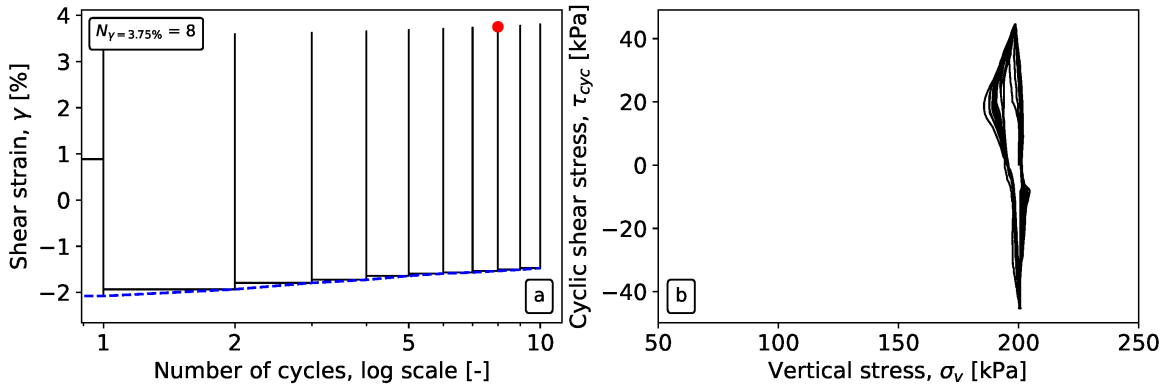

FIGURE 4.22: Test ID: LSR-200-C4. SCCDS test performed on a loose sample using a cyclic shear amplitude of 45 kPa. a. shear strain development wrt. number of cycles, b. Vertical stress response against cyclic shear stress.

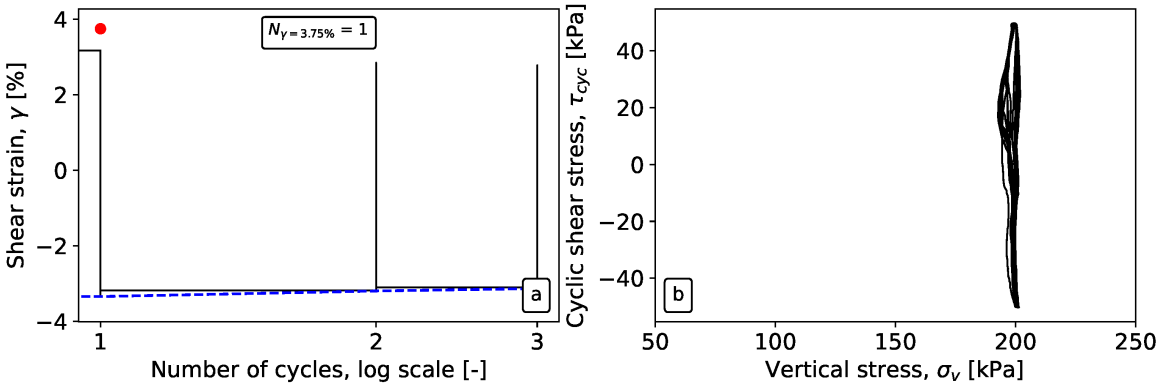

FIGURE 4.23: Test ID: LSR-200-C5. SCCDS test performed on a dense sample using a cyclic shear amplitude of 50 kPa. a. shear strain development wrt. number of cycles, b. Vertical stress response against cyclic shear stress.

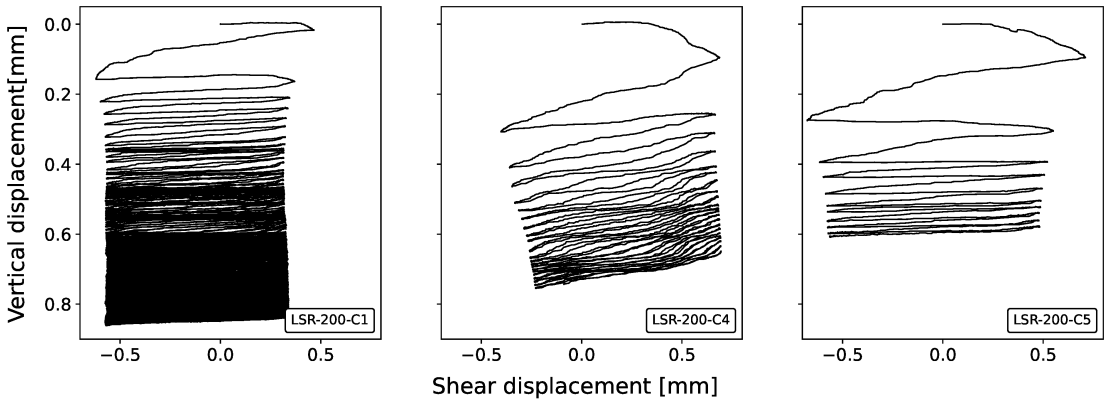

FIGURE 4.24: Response of the vertical extension with respect to the shear extension of the discussed tests.

4.3 Post-cyclic test results

After the cyclic stage, some samples were subjected to a strain-controlled monotonic shear test, under consolidated drained conditions, to determine the residual shear stress within the sample. The shear box was moved back to its neutral position (zero shear displacement) and the samples were reconsolidated back to 200 kPa. Table 4.3 presents the results of the post-cyclic test performed on some samples from program A and program B. The maximum shear displacement was set to 5 mm for both programs. Figure 4.25 shows the post-cyclic shear response of the samples from program A and exhibits no shear failure in the post-cyclic stage. Figure 4.27 shows the response of the samples from program B. It is observed that the dense samples have also not reached shear failure. The shear stress in both test programs show that a plateau is first reached around 50 kPa, before increasing further. This plateau is in the same range of the maximum shear amplitudes during the cyclic stage of the samples. This can be explained due to the fact that the shear box was moved to the zero shear displacement position prior to post-cyclic shearing. The volume changes during the post-cyclic stage is presented in Figure 4.26 for program A. Responses of program A show high contraction values after a slight dilative response at approximately 1.5 mm shear displacement. Interestingly, at this same position in Figure 4.25, the shear stresses increased further after the aforementioned plateau. On the other hand, the dense samples exhibited

the traditional contraction to dilation response until 2 mm shear displacement, as depicted in Figure 4.28. However, after further shearing the samples started to contract again.

TABLE 4.3: Post-cyclic shear test results.

			Post cyclic stage	
	Test#	**Test ID**	**Y/N?**	$\tau_{psmax}[kPa]$
Program A	1	LSRD-200-A1	Yes	170.6
	2	LSRD-200-A2	Yes	188.8
	3	LSRD-200-A3	Yes	170.9
Loose samples	4	LSRD-200-A4	Yes	195.13
	5	LSRD-200-A5	No	-
	6	LSRD-200-A6	Yes	107.14
Program B	1	DSRD-200-B1	Yes	140.96
	2	DSRD-200-B2	Yes	168.57
	3	DSRD-200-B3	No	-
Dense samples	4	DSRD-200-B4	No	-
	5	DSRD-200-B5	Yes	186.07
	6	DSRD-200-B6	Yes	207.6

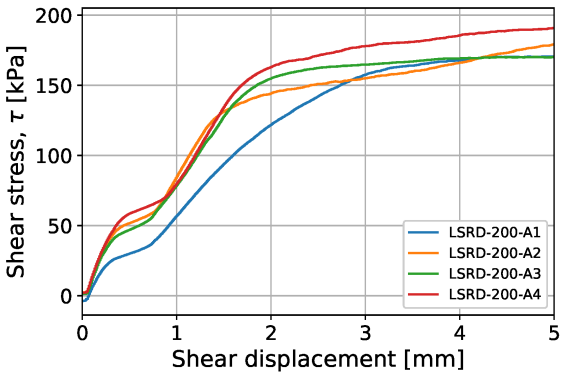

FIGURE 4.25: Post-cyclic shear test results performed on some samples from program A.

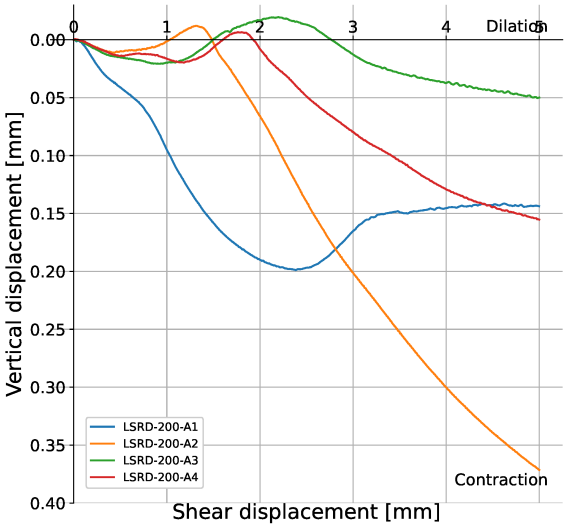

FIGURE 4.26: Volume change during post-cyclic loading in program A.

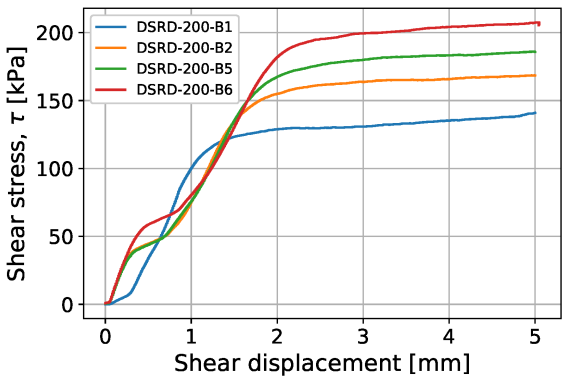

FIGURE 4.27: Post-cyclic shear test results performed on some samples from program A.

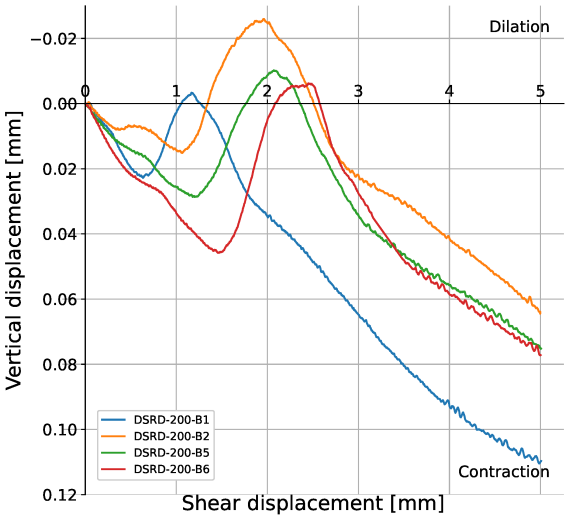

FIGURE 4.28: Volume change during post-cyclic shearing in program B.

4.4 Cyclic Resistance Ratio (CRR)

The cyclic resistance ratio is determined by relating the CSR and the $N_{\gamma=3.75\%}$ against each other in a semi-logarithmic plot as depicted in Figure 4.29. Plotting a power-fit line through these points, expresses this relationship in the form of a power-law function given by Equation 2.1. Table 4.4 presents the power-law functions obtained for the test programs A to C and the calculated CRR15 values using these equations. The CRR15 is the cyclic stress ratio needed to reach the liquefaction criteria within 15 cycles. To plot be able to plot the semi-logarithmic plots for programs A and C the test results of LSRD-200-A1 and LSR-200-C1, respectively, are used. In neither test is the liquefaction criteria reached, hence the maximum number of cycles is used to represent the CRR plots for these programs. Therefore, the CRR15 values calculated with their equations are considered to be conservative.

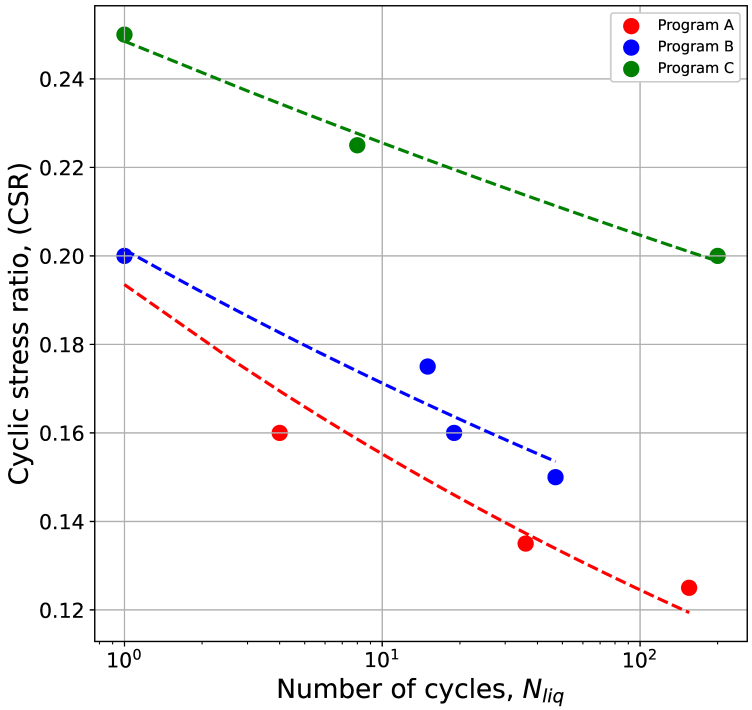

FIGURE 4.29: The cyclic resistance ratio (CRR) of fine-sand sand tailings determined for 15 cycles to reach the liquefaction criteria.

TABLE 4.4: Power law equations and its a & b parameters to determine the CSR needed to reach the liquefaction criteria within 15 cycles.

	CRR	**a**	**b**	**CRR15**
Program A	$0.1912N_{fl=3.75\%}{}^{-0.09}$	0.1912	0.072	0.15
Program B	$0.2021N_{fl=3.75\%}{}^{-0.072}$	0.2021	0.09	0.166
Program C	$0.2482N_{fl=3.75\%}{}^{-0.042}$	0.2482	0.042	0.221

Chapter 5

Discussion & Conclusion

The main objective of this thesis is to investigate how useful the direct shear test is to study the liquefaction behaviour of fine-sand tailings. For this purpose, stress-controlled cyclic direct shear tests were carried out on fine-sand tailings, received from the University of Western Australia (UWA), as means of a round-robin program. In this chapter, the findings from Chapter 4 are discussed and in the conclusion the research questions introduced in Chapter 1 are answered.

5.1 Discussion: Effects of relative density (D_r) on cyclic direct shear tests

The influence of relative density (Dr) is investigated by comparing the results of program A and program B. For a better comparison, the tests with the same CSR values are compared, namely LSRD-200-(A3, A4, A5) and DSRD-200-(B1, B2, B3), with CSR values 0.15, 0.16 and 0.175, respectively. During the consolidation stage, the loose samples (Dr = 20%) from program A underwent a higher degree of settlement at the end of consolidation (EOC) than the dense samples (Dr = 65%) from program B as depicted in Figure 5.1. The horizontal shear displacement during the shear bias stage, shown in Figure 5.2 is also observed to be higher for the loose samples. There is also a relatively small amount of additional settlement observed during this stage for tests of program A, shown in Figure 5.3. Program B also shows almost no change in settlement, except for DSRD-200-B2, which underwent an additional 0.6 mm settlement. A possible reason for this could be the soil was not evenly distributed during the sample preparation, leading to settlements different to the other samples.

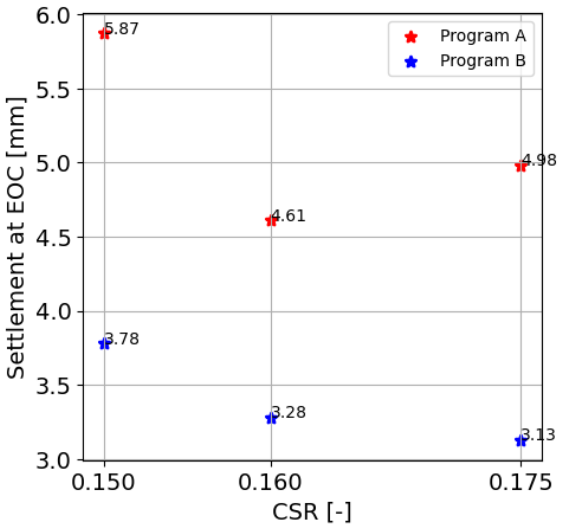

FIGURE 5.1: Settlement at EOC stage.

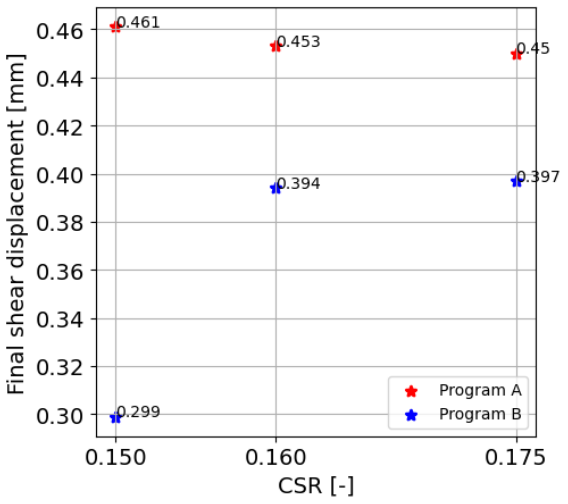

FIGURE 5.2: Horizontal displacement at end of shear bias stage.

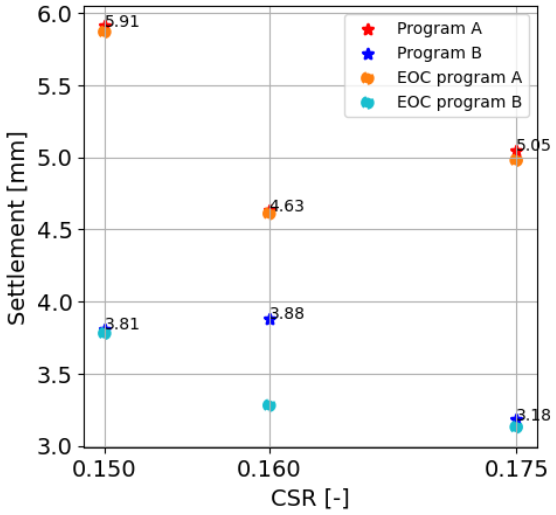

FIGURE 5.3: Settlement at end of shear bias stage.

5.2 Discussion: Effects of drained shear bias (τ_α) on cyclic direct shear tests

The effects of drained shear bias is investigated by looking at the results of program A and program C. Specifically, test LSRD-200-A6 and LSR-200-C1 are compared. Comparing the cyclic shear test results from Figure 4.14 and Figure 4.21 with the same CSR, LSRD-200-A6 reached the liquefaction criteria of $\gamma = 3.75\%$ in just 1 cycle, whereas LSR-200-C1 did not meet this criteria within 200 cycles. The overall change in void ratio (e_c) at EOC was also noted to be higher for the samples of program A, compared to program C, as seen in Figure 5.4. Despite the higher void ratio's, the tests of program A reached the liquefaction criteria with lower CSR values, indicating that the drained shear bias, which simulates sloping ground conditions, is more susceptible to liquefaction than level ground condition. The difference in void ratio observed in this Figure may lie in the sample preparation stage due to the difficulty of preparing loose samples manually.

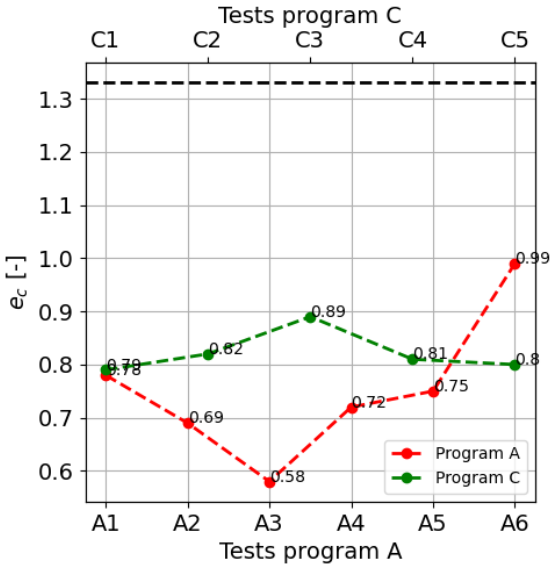

FIGURE 5.4: Comparison of the consolidated void ratio between tests of program A and C.

5.3 Discussion:Response of post-cyclic shear stress

After the cyclic shear test, some samples were subjected to strain-controlled post-cyclic shearing to determine how much residual shear strength the sample still has. The post-cyclic shear stresses reached by the loose samples in program A lies between 170 kPa and 195 kPa, as depicted in Figure 5.5. The stresses of the dense samples of program B show a consistent increase in residual shear stress with increasing CSR. A reason for this may lie in the number of cyclic loading the samples underwent. As previously mentioned, higher CSR required lower number of cycles to reach $N_{\gamma=3.75\%}$. This means that in the samples with higher CSR values still had a higher residual shear strength present. The results of program A shows a fluctuating shear response with respect to CSR, making it difficult to analyse this data.

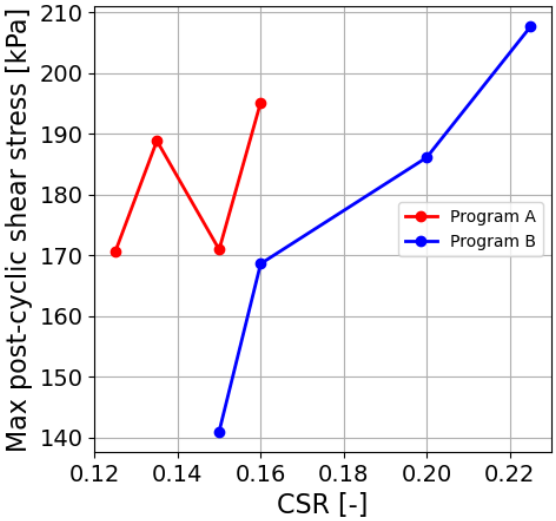

FIGURE 5.5: Comparison between the maximum post-cyclic shear stress of program A and program B.

5.4 Conclusion

As this thesis attempts to study the cyclic shear response of fine-sand tailings with the use of a direct shear box, it is not possible to fully quantify the results, thus the conclusions of this study are given qualitatively. Following the discussion, the main research question **"How useful is the cyclic direct shear test to study the liquefaction response of fine-sand tailings?"** can be answered with the help of the sub-questions, previously defined in Chapter 1. The answers to these sub questions are as follows:

1. **What is the influence of relative density to reach liquefaction criteria under cyclic direct shear loading?**
   As evident from Table 4.2, loose samples from program A are more sensitive to lower CSR values compared to program B. In both cases, increasing the CSR led to more insensitive results. This can be seen in tests LSRD-200-A3, A4, A5, where $\gamma = 3.75\%$ is reached in 4 cycles and for tests DSRD-200-B4, B5, B6 this criteria was reached within 1 cycle. Following these results, it can be concluded that for the application of cyclic direct shear test on fine-sand tailings, dense samples deliver a more sensitive response to the liquefaction criteria for low CSR values compared to loose samples. Additionally, according to the CRR results, depicted in Figure 4.29, the dense samples exhibited approximately 9.6% more cyclic resistance compared to the loose sample from program A, thus concluding that denser soils have a higher resistance ratio, compared to loose soils.

2. **How does the drained shear bias influence the cyclic shear response?**
   Following the discussion in Chapter 5.2, it can be said that the application of the drained shear bias has a major influence on the cyclic shear response. The application of τ_α in program A resulted in the tests reaching the liquefaction criteria with lower CSR values, whereas tests from program C required a much higher CSR value. This is also reflected in Figure 4.29 where program C has around 32% higher cyclic resistance than program A. In conclusion, it can be said that the application of drained shear bias results in lower CSR values needed to reach liquefaction. In other words, level ground conditions have a higher resistance to liquefaction than the sloping ground conditions.

3. **How does the fine sand tailings respond when subjected to post-cyclic loading?**
   Post-cyclic test results of program B showed that the residual shear stress increased with increasing CSR, shown in Figure 5.5. Looking at the volume changes during each stages of the tests, it is observed that the samples kept on contracting despite having a high relative density. During the cyclic stage, tests with higher CSR underwent higher shear displacement. It can thus be argued that the higher residual shear stress resulted from the additional densification during the cyclic stage. All samples also exhibited strain hardening behaviour (Figures 4.25 & 4.27) and achieved a much higher maximum shear stress than the monotonic shear test (Test ID: SR-200-M) performed under 200 kPa vertical stress, presented in Chapter 4.1. On average, the loose samples achieved 3% higher post-cyclic shear strain. Figures 4.26 & 4.28 displayed further contractive response of the samples after exhibiting a dilative response. This contractive response explains the strain hardening behaviour and could be the result of the constant normal load condition.

Overall conclusion: The use of the cyclic direct shear test method to investigate the cyclic shear response of fine-sand tailings gave similar results as expected from a theoretical stance. In short, denser soils and soils tested for level ground conditions both have a higher cyclic resistance compared to their counter parts. The advantages of this test methods are:

1. It gave some insight on the plastic deformation accumulation of the tailings under repeated cyclic loading. Results show a slight increase in plastic deformation with increasing τ_{cyc}.

2. The constant normal stress condition gave some useful strength data of the tailings during the post-cyclic stage. This data can provide some information for tackling certain engineering problems, such as studying slope stability.

However, this study also shed light to some limitations, which prevented in obtaining highly reliable data:

1. A major factor in the study of liquefaction is the influence of pore-water pressure. The aim of this study was to perform cyclic direct shear test under partially drained conditions. The main contributor for this test program was the frequency. Unfortunately due to incorrect application of this frequency input of the used license, the tests were not performed optimally.

2. The manual preparation of loose samples for a direct shear test is fairly difficult and inconsistent. On the other hand, dense samples are easier to prepare, and its tests yielded more consistent results.

Although, this study showed that in terms of determining the cyclic resistance ratio, the stress-controlled direct shear test deliver similar results as cyclic direct simple shear tests, the liquefaction criteria of $\gamma = 3.75\%$ is reached only due to the plastic shear strain development, also known as strain softening.

Chapter 6

Recommendations

The study and analysis of this thesis objective showed that there is much room for improvement. This Chapter highlights some recommendations which can help improve the study of liquefaction using a direct shear apparatus.

6.1 Recommendations on the improvement of the direct shear device

As demonstrated, the direct shear apparatus from Wille Geotechnik is very much capable to conduct stress-controlled cyclic direct shear tests. However, there are some options absent, which prevents from computing optimal results. Adding the following controls/options may help further improve the application of this method.

1. Changing the direction of the applied cyclic shear stress relatively quicker during the cyclic stage and thus being able to implement an accurate frequency of the cycles.
2. Being able to conduct the tests under constant volume. This causes the volume of the sample to remain constant while the vertical stress changes. This change in stress is equivalent to pore pressure generated according to Hanzawa et al., 2007.
3. If the tests require post-cyclic shear test, it is recommended to add the post-cyclic stage in the same test license as the stress-controlled cyclic test.

6.2 Recommendations on cyclic shear test

To further build on the tests presented in this thesis, some additional studies are recommended:

1. Performing some cyclic direct shear tests on dense samples with the application of drained shear bias, similar to program C, can shed more light to the influence the drained shear bias by comparing its effects on dense and loose samples.
2. Conducting the cyclic tests with different vertical stresses can further broaden the analysis on the influences of constant normal load, consolidated void ratio, and relative density on the study of liquefaction. It can furthermore help with studying its effects in plastic strain development.
3. It is further recommended to conduct some cyclic direct simple shear tests on the same material. This can help greatly in comparing both methods and further solidifying the reliability and use of direct shear test to study liquefaction.

Bibliography

Al-Douri, Riadh H. et al. (1992). "Static and cyclic direct shear tests on carbonate sands". In: *Geotechnical Testing Journal* 15.2, pp. 138–157. ISSN: 01496115. DOI: 10.1520/gtj10236j.

Amini, F. et al. (2000). "Liquefaction Testing of Stratified Silty Sands". In: *Journal of Geotechnical and Geoenvironmental Engineering* 126.3, pp. 208–217. DOI: 10.1061/(ASCE)1090-0241(2000)126:3(208).

Andersen, Knut H. (2009). "Bearing capacity under cyclic loading -offshore, along the coast, and on land. The 21st Bjerrum Lecture presented in Oslo, 23 November 2007". In: *Canadian Geotechnical Journal* 46.5, pp. 513–535. ISSN: 00083674. DOI: 10.1139/T09-003.

ASTMD3080 (2011). "Standard Test Method for Direct Shear Test of Soils Under Consolidated Drained Conditions". In: *ASTM International* D3080-11.D3080-11, pp. 343–351. DOI: 10.1520/D3080.

ASTMD4253 (2016). *ASTM D4253 - 16e1 Standard Test Methods for Maximum Index Density and Unit Weight of Soils Using a Vibratory Table*. URL: https://www.astm.org/Standards/D4253.htm.

ASTMD4254 (2016). *ASTM D4254-16 Standard Test Methods for Minimum Index Density and Unit Weight of Soils and Calculation of Relative Density* 1. DOI: 10.1520/D4254-16.2.

ASTMD555014 (2014). "Standard Test Methods for Specific Gravity of Soil Solids by Water Pycnometer 1". In: pp. 1–8. DOI: 10.1520/D0854-10..

Boulanger, Ross W. et al. (1995). "Liquefaction of sand under bidirectional monotonic and cyclic loading". In: *Journal of Geotechnical Engineering* 121.12, pp. 870–878. ISSN: 0733-9410. DOI: 10.1061/(ASCE)0733-9410(1995)121:12(870).

Cabalar, Ali Firat et al. (2013). "Strength of various sands in triaxial and cyclic direct shear tests". In: *Engineering Geology* 156, 92–102. DOI: 10.1016/j.enggeo.2013.01.011.

Casagrande, Arthur (1975). "Liquefaction and cyclic deformation of sands: A critical review". In: *Proceedings of the Panamerican Conference on Soil Mechanics and Foundation Engineering* 88, pp. 79–133.

Finn, W.D.L. et al. (1977). *Liquefaction potential from drained constant volume cyclic simple shear tests*. URL: http://www.iitk.ac.in/nicee/wcee/article/6_vol3_2157.pdf.

Frost, J D et al. (2003). "A critical assessment of the moist tamping technique". In: *Geotechnical Testing Journal* 26.1, pp. 57–70. ISSN: 01496115. DOI: 10.1520/gtj11108j. URL: www.astm.org.

Hanzawa, Hideo et al. (2007). "A comparative study between the NGI direct simple shear apparatus and the Mikasa direct shear apparatus". In: *Soils and Foundations* 47.1, pp. 47–58. ISSN: 00380806. DOI: 10.3208/sandf.47.47.

Ingabire, Edouardine-pascale (2019). "Influence of fines content on cyclic resistance and residual strength of Base Metal Tailings". In: p. 299.

Ishihara, KENJI et al. (1980). "Cyclic Strength Characteristics Of Tailings Materials". In: *SOILS AND FOUNDATIONS* 20.4, pp. 127–142. DOI: 10.3208/sandf1972.20.4_127.

Jiang, M. J. et al. (2003). "An efficient technique for generating homogeneous specimens for DEM studies". In: *Computers and Geotechnics* 30.7, pp. 579–597. ISSN: 0266352X. DOI: 10.1016/S0266-352X(03)00064-8.

Ke, Xiqun et al. (2019). "A new failure criterion for determining the cyclic resistance of low-plasticity fine-grained tailings". In: *Engineering Geology* 261, p. 105273. ISSN: 0013-7952. DOI: https://doi.org/10.1016/j.enggeo.2019.105273. URL: https://www.sciencedirect.com/science/article/pii/S0013795218310500.

Khashila, Marwan et al. (2021). "Liquefaction resistance from cyclic simple and triaxial shearing: a comparative study". In: *Acta Geotechnica* 16.6, pp. 1735–1753. ISSN: 18611133. DOI: 10.1007/s11440-020-01104-6.

Konstadinou, M. et al. (2020). "The Influence of Apparatus Stiffness on the Results of Cyclic Direct Simple Shear Tests on Dense Sand". In: *Geotechnical Testing Journal* 44.5, p. 20190471. DOI: 10.1520/gtj20190471.

Ladd, RS et al. (1978). "Preparing Test Specimens Using Undercompaction". In: *Geotechnical Testing Journal* 1.1, p. 16. ISSN: 01496115. DOI: 10.1520/gtj10364j.

Lottermoser, Bernd G. (2010). "Tailings". In: *Mine Wastes: Characterization, Treatment and Environmental Impacts*. Berlin, Heidelberg: Springer Berlin Heidelberg, pp. 205–241. ISBN: 978-3-642-12419-8. DOI: 10.1007/978-3-642-12419-8_4. URL: https://doi.org/10.1007/978-3-642-12419-8_4.

Randolph, Mark et al. (2017). *Offshore geotechnical engineering*, pp. 1–528. ISBN: 9781351988919. DOI: 10.1201/9781315272474.

Salamatpoor, Sina et al. (2014). "Evaluation of Babolsar Sand Behaviour by Using Static Triaxial Tests and Comparison with Case History". In: *Open Journal of Civil Engineering* 04.03, 181–197. DOI: 10.4236/ojce.2014.43016.

Sanin, Maria Victoria (2005). "Cyclic shear loading response of Fraser River Delta silt". PhD thesis. University of British Columbia. DOI: http://dx.doi.org/10.14288/1.0063358. URL: https://open.library.ubc.ca/collections/ubctheses/831/items/1.0063358.

— (2010). "Cyclic shear loading response of Fraser River delta silt". PhD thesis. University of British Columbia. DOI: http://dx.doi.org/10.14288/1.0062865. URL: https://open.library.ubc.ca/collections/ubctheses/24/items/1.0062865.

Seidalinova, Ainur (2014). "Monotonic and cyclic shear loading response of fine-grained gold tailings". PhD thesis. University of British Columbia. DOI: http://dx.doi.org/10.14288/1.0167423. URL: https://open.library.ubc.ca/collections/ubctheses/24/items/1.0167423.

Silva Rotta, Luiz Henrique et al. (2020). "The 2019 Brumadinho tailings dam collapse: Possible cause and impacts of the worst human and environmental disaster in Brazil". In: *International Journal of Applied Earth Observation and Geoinformation* 90.April, p. 102119. ISSN: 03032434. DOI: 10.1016/j.jag.2020.102119. URL: https://doi.org/10.1016/j.jag.2020.102119.

Sivathayalan, S. (1994). "Static, cyclic and post liquefaction simple shear sesponse of sands". In: December, p. 154.

Ulmer, Kristin et al. (2019). "Quality assurance for cyclic direct simple shear tests for evaluating liquefaction triggering characteristics of cohesionless soils Liquefaction Risk Mitigation View project Resilient and Sustainable Buildings: Performance-Based Engineering View project". In: *Proceedings of the XVII ECSMGE* September. DOI: 10.32075/17ECSMGE-2019-0470. URL: https://www.researchgate.net/publication/335700604.

Verma, P. et al. (2015). "Some observations on the effect of initial static shear stress on cyclic response of natural silt from Lower Mainland of British Columbia". In: *Proceedings of the 6th International Conference on Earthquake Geotechnical Engineering* November, 1–4 November, 9pp.

Verma, Priyesh (2019). "Monotonic and cyclic shear loading response of natural silts from British Columbia, Canada". In: September. URL: http://hdl.handle.net/2429/52356.

Wijewickreme, Dharma et al. (2005). "Cyclic shear response of fine-grained mine tailings". In: *Canadian Geotechnical Journal* 42.5, 1408–1421. DOI: 10.1139/t05-058.

Appendix A

Sample preparation procedure

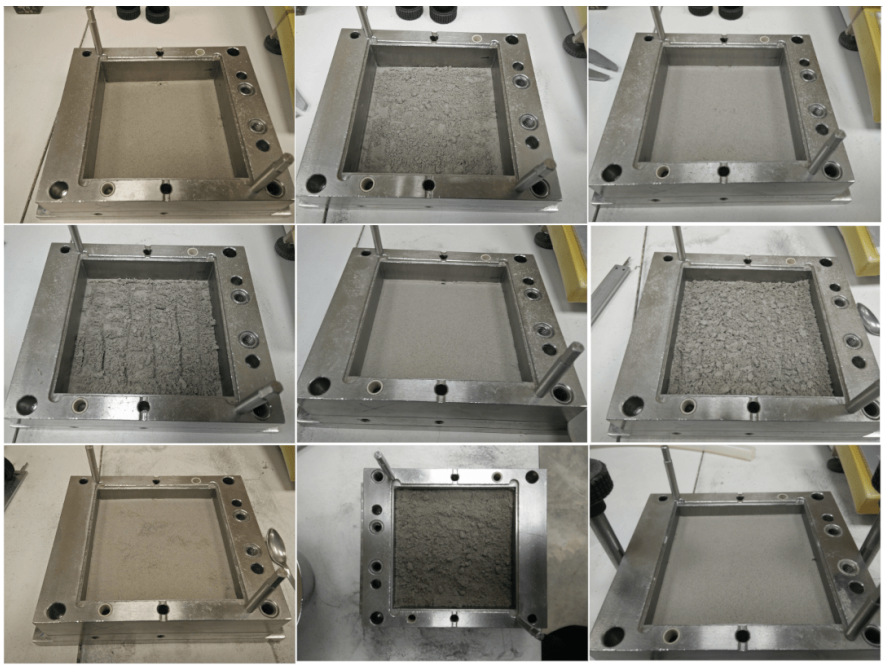

FIGURE A.1: The sample preparation steps of a dense sample in 5 layers. Before proceeding to place the subsequent sub-layer, the surface is scarified to ensure an uniform connection between each layer.

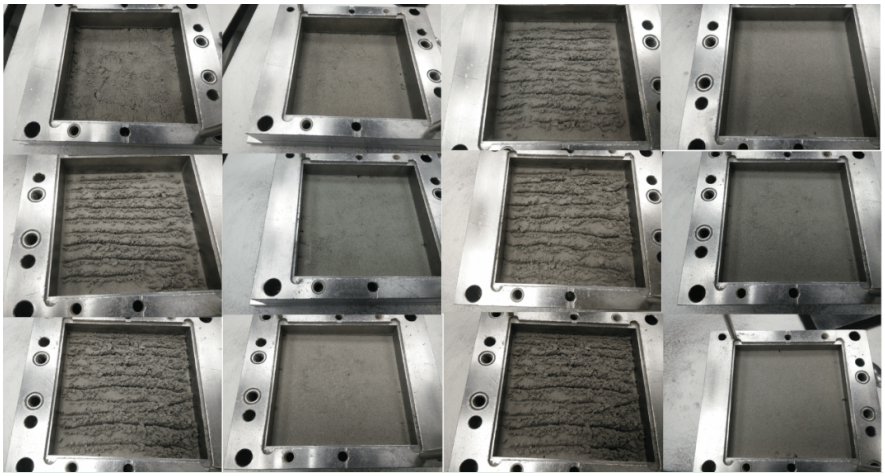

FIGURE A.2: Sample preparation steps of a loose sample constructed in 7 layers. Similarly to the dense sample, each sub-layer is scarified before placing the next sub-layer.

Appendix B

Additional cyclic direct shear results

In this appendix the additional plots of the cyclic shear results from Chapter 4 are found.
Test results from program A.

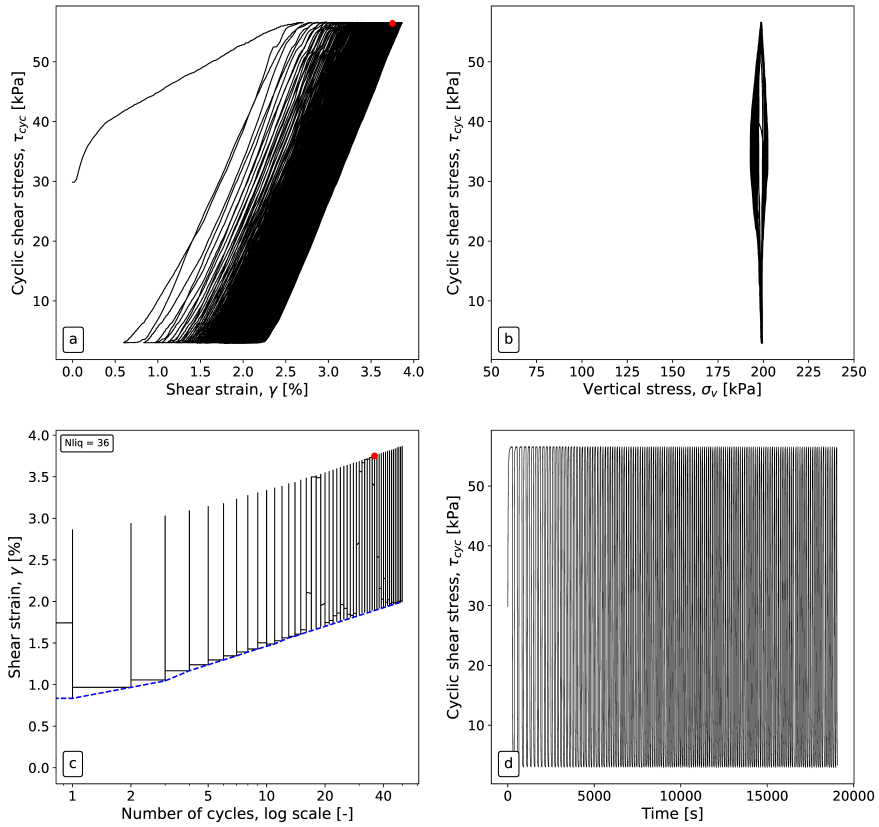

FIGURE B.1: Test ID: LSRD-200-A2. SCCDS test performed on a loose sample using a cyclic shear amplitude of 27 kPa. a. Stress-strain response, b. Vertical stress behaviour against cyclic shear stress, c. shear strain development, d. Cyclic shear stress response against time.

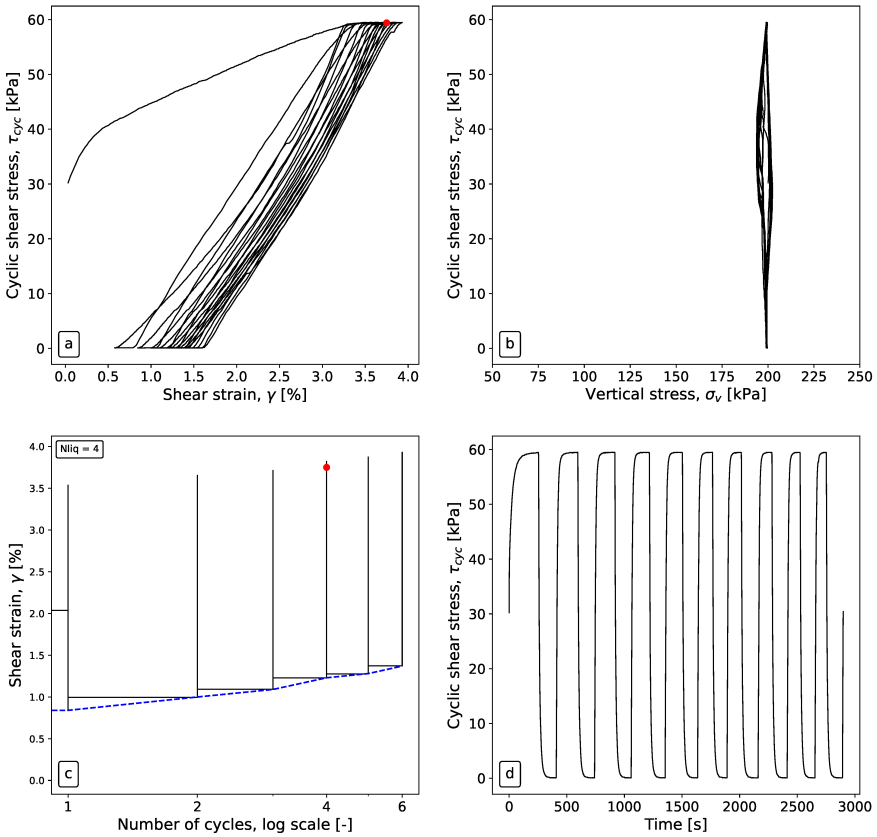

FIGURE B.2: Test ID: LSRD-200-A3. SCCDS test performed on a loose sample using a cyclic shear amplitude of 30 kPa. a. Stress-strain response, b. Vertical stress behaviour against cyclic shear stress, c. shear strain development, d. Cyclic shear stress response against time.

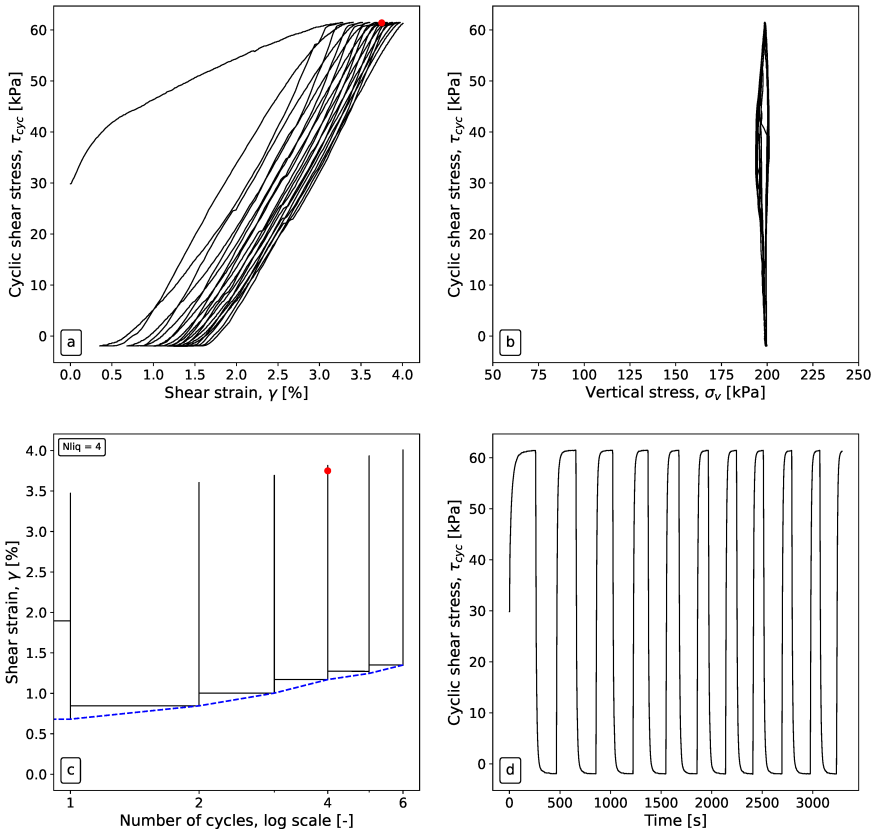

FIGURE B.3: Test ID: LSRD-200-A4. SCCDS test performed on a loose sample using a cyclic shear amplitude of 32 kPa. a. Stress-strain response, b. Vertical stress behaviour against cyclic shear stress, c. shear strain development, d. Cyclic shear stress response against time.

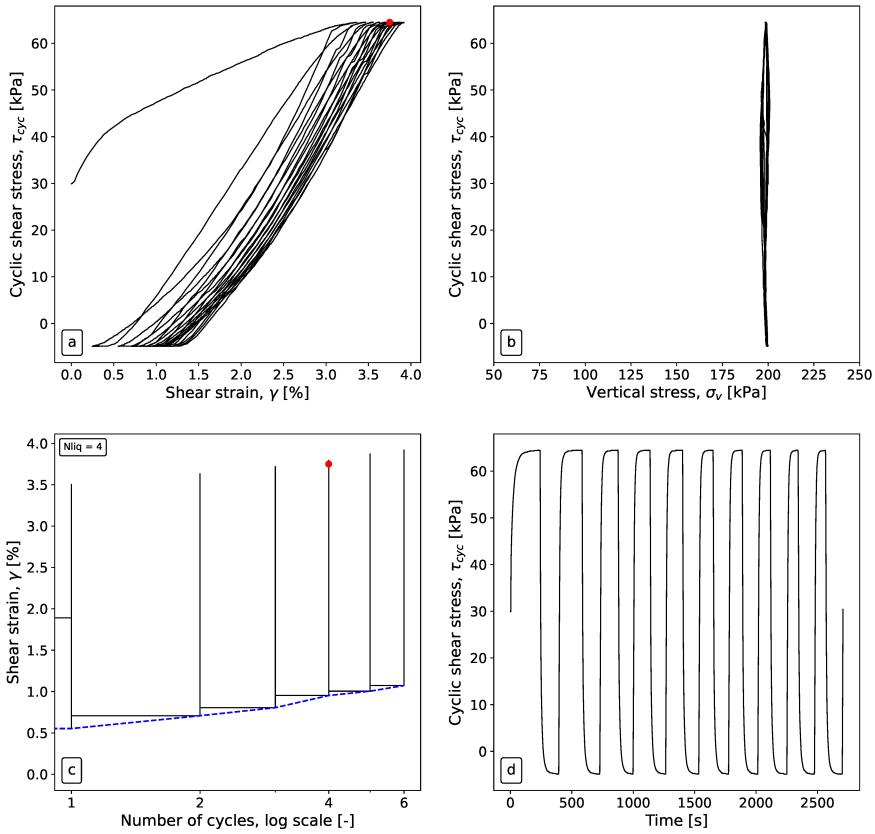

FIGURE B.4: Test ID: LSRD-200-A5. SCCDS test performed on a loose sample using a cyclic shear amplitude of 35 kPa. a. Stress-strain response, b. Vertical stress behaviour against cyclic shear stress, c. shear strain development, d. Cyclic shear stress response against time.

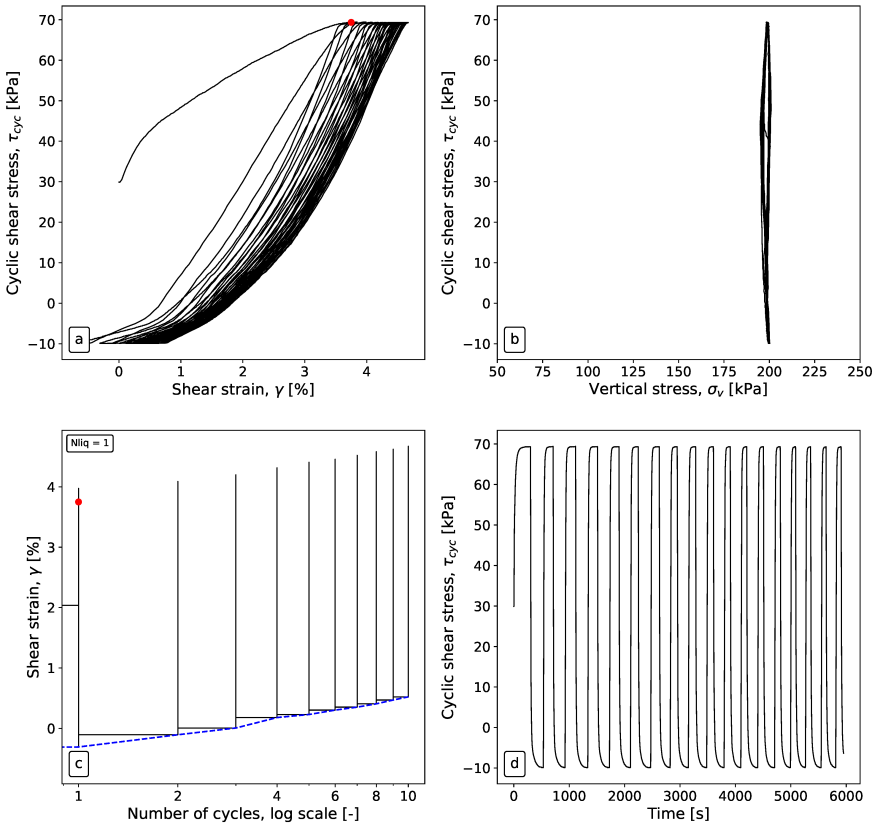

FIGURE B.5: Test ID: LSRD-200-A6. SCCDS test performed on a loose sample using a cyclic shear amplitude of 40 kPa. a. Stress-strain response, b. Vertical stress behaviour against cyclic shear stress, c. shear strain development, d. Cyclic shear stress response against time.

Test results from program B.

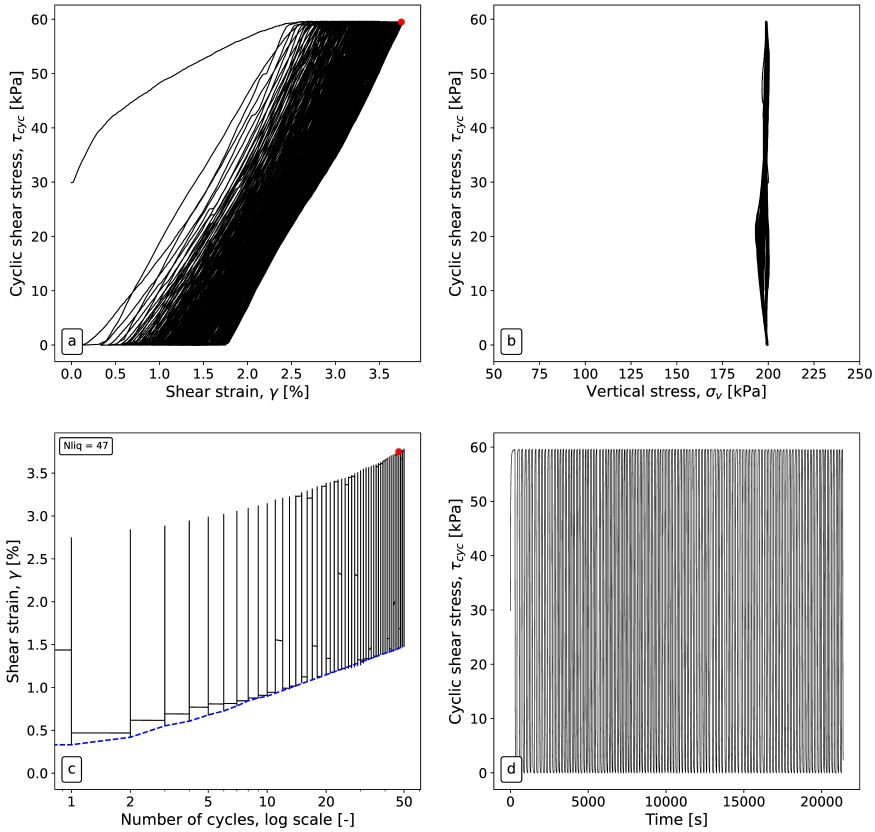

FIGURE B.6: Test ID: LSRD-200-A6. SCCDS test performed on a loose sample using a cyclic shear amplitude of 30 kPa. a. Stress-strain response, b. Vertical stress behaviour against cyclic shear stress, c. shear strain development, d. Cyclic shear stress response against time.

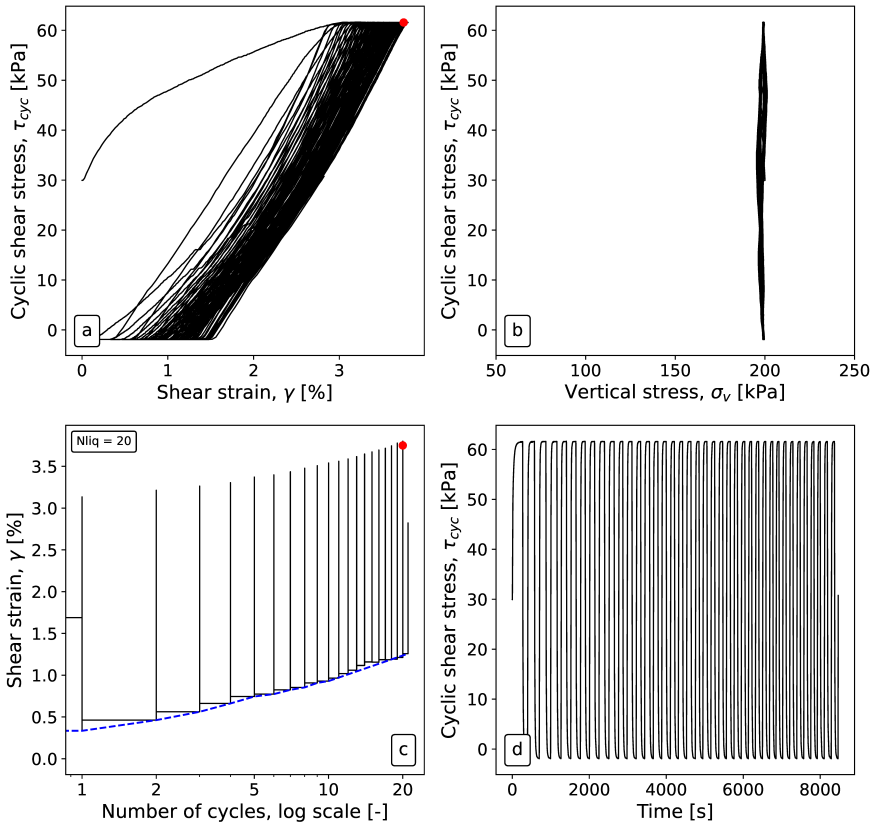

FIGURE B.7: Test ID: LSRD-200-B2. SCCDS test performed on a loose sample using a cyclic shear amplitude of 32 kPa. a. Stress-strain response, b. Vertical stress behaviour against cyclic shear stress, c. shear strain development, d. Cyclic shear stress response against time.

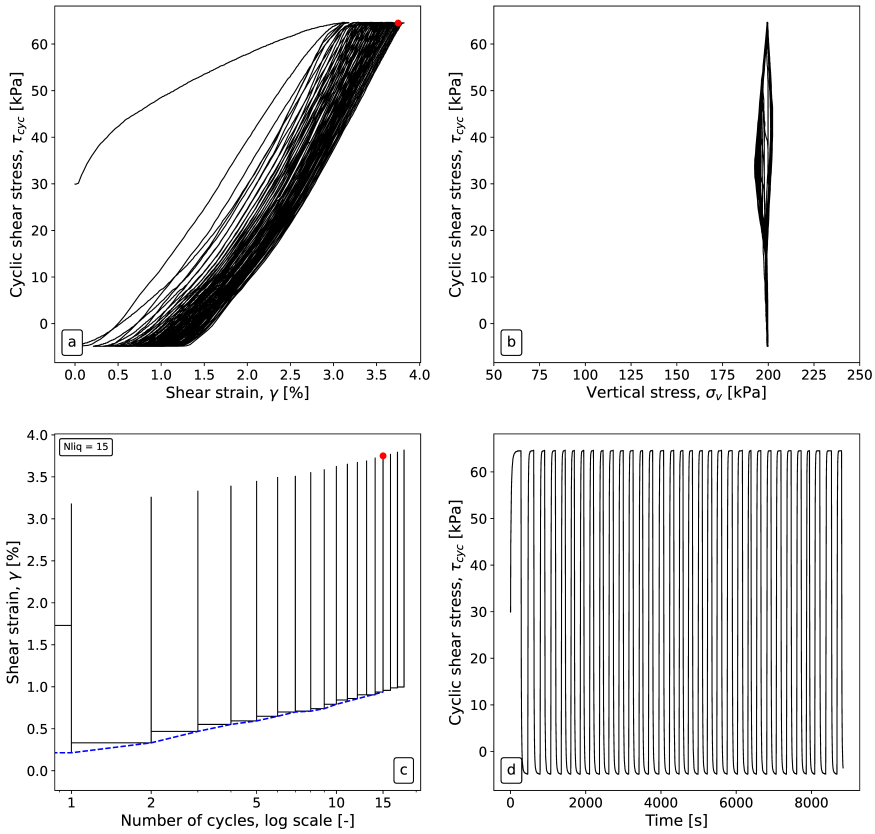

FIGURE B.8: Test ID: LSRD-200-B3. SCCDS test performed on a loose sample using a cyclic shear amplitude of 35 kPa. a. Stress-strain response, b. Vertical stress behaviour against cyclic shear stress, c. shear strain development, d. Cyclic shear stress response against time.

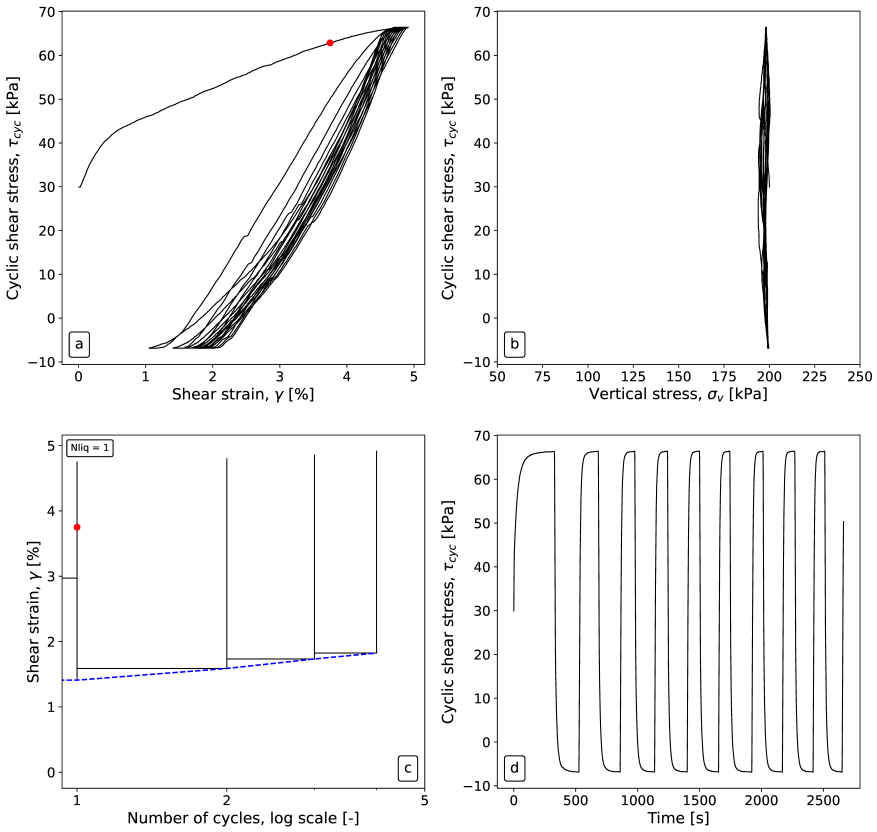

FIGURE B.9: Test ID: LSRD-200-B4. SCCDS test performed on a loose sample using a cyclic shear amplitude of 37 kPa. a. Stress-strain response, b. Vertical stress behaviour against cyclic shear stress, c. shear strain development, d. Cyclic shear stress response against time.

Test results from program C.

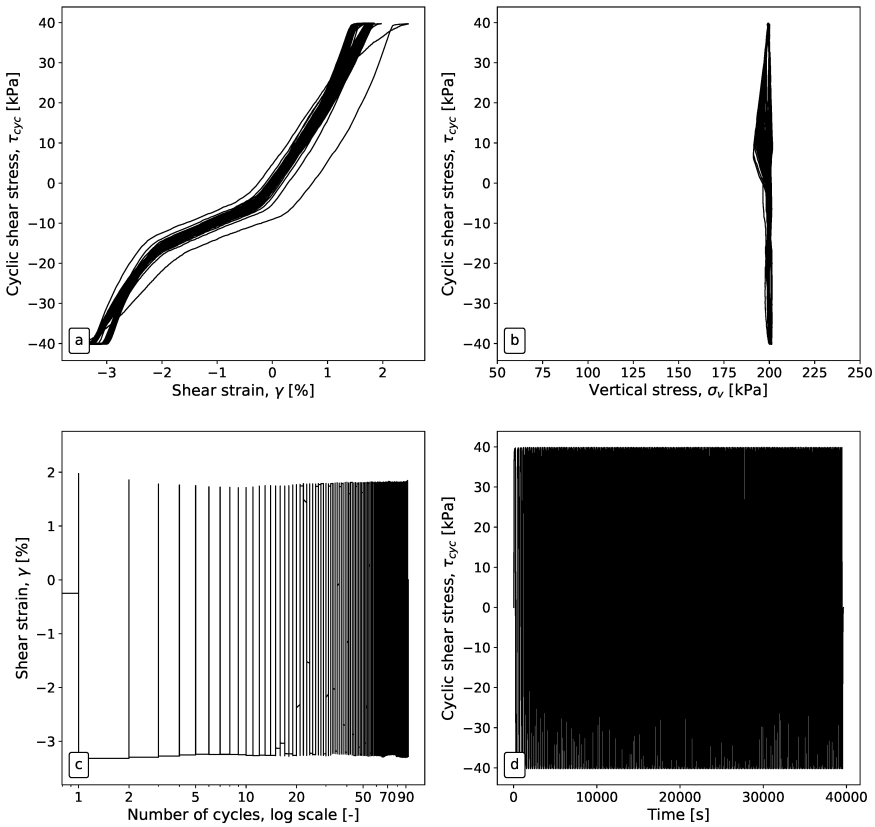

FIGURE B.10: Test ID: LSR-200-C1. SCCDS test performed on a loose sample using a cyclic shear amplitude of 40 kPa. a. Stress-strain response, b. Vertical stress behaviour against cyclic shear stress, c. shear strain development, d. Cyclic shear stress response against time.

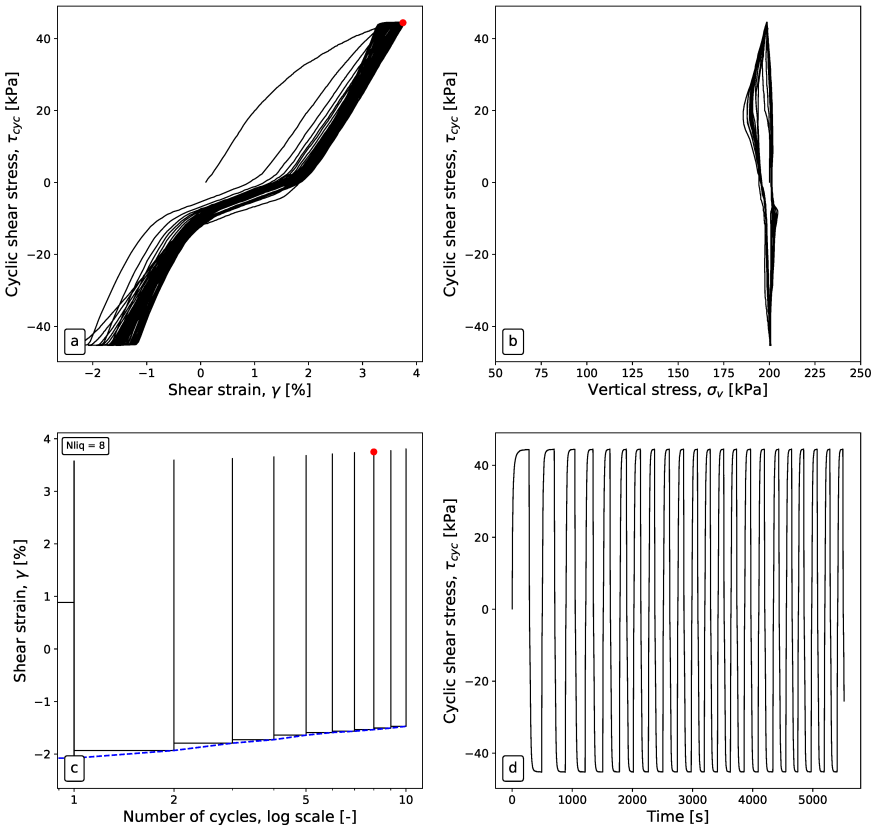

FIGURE B.11: Test ID: LSRD-200-C4. SCCDS test performed on a loose sample using a cyclic shear amplitude of 45 kPa. a. Stress-strain response, b. Vertical stress behaviour against cyclic shear stress, c. shear strain development, d. Cyclic shear stress response against time.

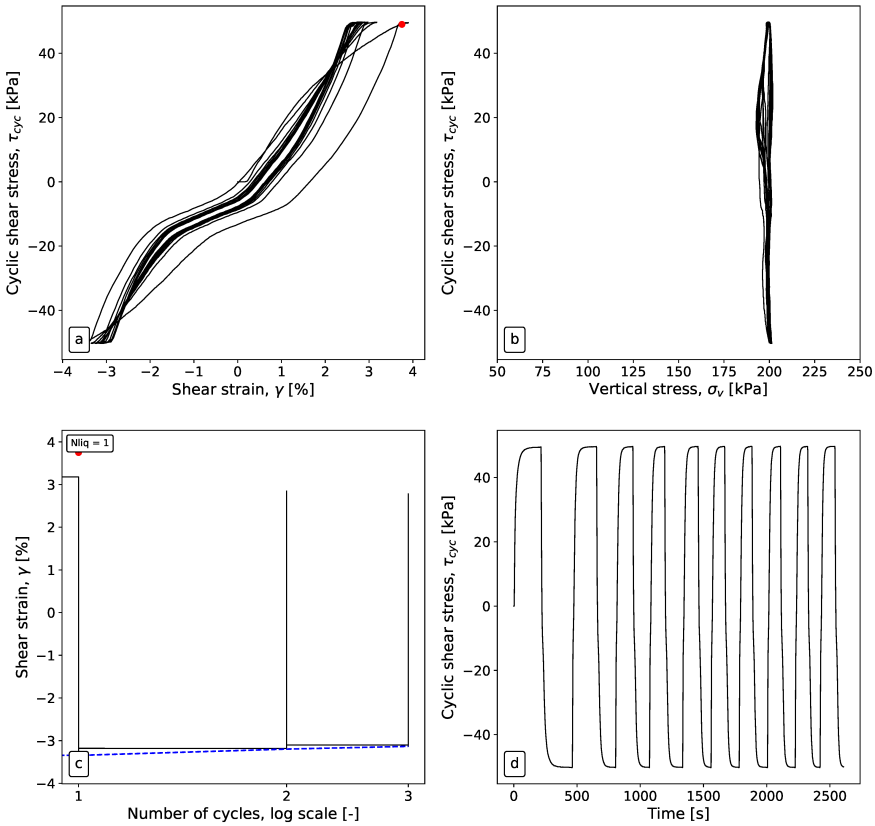

FIGURE B.12: Test ID: LSRD-200-C5. SCCDS test performed on a loose sample using a cyclic shear amplitude of 50 kPa. a. Stress-strain response, b. Vertical stress behaviour against cyclic shear stress, c. shear strain development, d. Cyclic shear stress response against time.